www.project-foci.eu

Co-funded by the European Union

UK Research and Innovation

Horizon Europe

(HORIZON-CL5-2021-D1-01)

Non-CO2 Forcers and their Climate, Weather, Air Quality and Health Impacts

FOCI

Deliverable 1.3

Report on the results from the model representation of physicochemical properties and feedback mechanisms of anthropogenic aerosols and non-CO2 gaseous species.

Grant agreement No 101056783

Grant Agreement No.	101056783	
Project acronym	FOCI	
Project full title	Non-CO2 Forcers and their Climate, Weather, Air Quality and Health Impacts	
Call	HORIZON-CL5-2021-D1-01	
Deliverable name	D1.3 Report on the results from the model representation of physicochemical properties and feedback mechanisms of anthropogenic aerosols and non-CO2 gaseous species.	
WP contributing to the deliverable	WP1	
Task producing the deliverable	Task 1.3	
Type	X	Report
		Prototype
		Demonstrator
		Other: Data
Dissemination level	X	Public
		Sensitive
		UE/EU-Restricted
Due date of deliverable	Month 30	
Actual submission date	Month 30	
Lead beneficiary	FMI	
Author(s)	Hector Navarro-Barboza (BSC), Vincenzo Obiso (BSC), Marco Pandolfi (CSIC), Oriol Jorba (BSC), Aino Ovaska (UHEL), Pauli Paasonen (UHEL), Tero Mielonen (FMI), Akash Deshmukh (FMI), Risto Makkonen (FMI), Tommi Bergman (FMI)	
Other Contributor(s)		
Reviewer(s)	Sergey Gromov	
Keywords	FOCI, deliverables, report	

ACKNOWLEDGEMENTS

This project has been co-funded by the European Union with funding from the European Union's Horizon Europe research and innovation programme under grant agreement No. 101056783 and from UKRI under the UK Government's Horizon Europe Guarantee (UKRI Reference Numbers: 10040465, 10053814 and 10050799).

Version	Date	Modified by	Comments
1.0	19.6.2025	Tommi Bergman	First version
	08.08.2025	Sergey Gromov	Internal review
1.1	15.8.2025	Tommi Bergman	Corrections from internal review

	Name	Date
Verification Final Draft by WP leaders	Marco Pandolfi (CSIC), Tommi Bergman (FMI)	18 August 2025
Check before upload by project Coordinator	Tomas Halenka (CU)	19 August 2025

TABLE OF CONTENTS

EXECUTIVE SUMMARY

This document is the deliverable "D1.3: Report on the results from the model representation of physicochemical properties and feedback mechanisms of anthropogenic aerosols and non-CO2 gaseous species." for the European Union project "FOCI: Non-CO2 Forcers and their Climate, Weather, Air Quality and Health Impacts" (hereinafter also referred to as FOCI, project reference: 101056783).

Here we document the work done on the Task 1.3 to analyse observations and models for the sensitivity simulations with OpenIFS, EC-Earth3, MONARCH and WRF models.

We present initial test simulations to give first evaluation of HAM-M7 aerosol scheme implementation within OpenIFS. For EC-Earth3, we have studied the impact of new emission inventory of brown carbon for its radiative effect. Furthermore, a machine learning model for cloud droplet number concentration prediction developed for efficient application in climate models has been evaluated in offline mode. Evaluation of HAM-M7 implementation showed some agreement with literature, while removal of aerosols still has issues related to convective wet deposition and lacking new particle formation. Brown carbon (BrC) impact on radiation was found to be limited globally, while it may have a pronounced effect locally in emission hot spots such as China.

In regional modelling, a set of configurations of WRF was tested and one configuration was selected for long-term simulations. Moreover, MONARCH chemical transport model simulations showed agreement in terms of BrC absorption variability. However, these simulations revealed uncertainties in emissions and ageing processes.

Future work should aim for improving BrC parameterisations and emission inventories to reduce the uncertainties. For the EC-Earth3 and OpenIFS, model development and evaluation are to be continued within the project in WP3 to remedy issues with aerosol removal efficiency and further evaluating the BrC contribution.

CONTRIBUTION TO THE FOCI OBJECTIVES

The Deliverable 1.3 initiates the model development analysis with sensitivity simulations and provides feedback for other WPs on model development and simulation setups for regional scale simulations. In practice the work provides the following:

1. Initial test simulations using OpenIFS-HAM-M7 to guide the development work done in WP3.
2. Examine and analyze the sensitivity simulations using EC-Earth3 to evaluate the impacts on model performance for future implementations in WP3 or beyond.
    a. Examine and evaluate the role of brown carbon on the radiation.
    b. Examine the influence of methyl sulfonic acid on particle formation.
3. Offline evaluation of machine learning-based cloud droplet model for future implementation in EC-Earth4/OpenIFS.
4. Evaluate and provide feedback on the optimal simulation setup for WRF.
5. Evaluation of the brown carbon modelling using a chemical transport model MONARCH for guidance on how to improve the model description of Brown carbon.

1. INTRODUCTION

Understanding the physicochemical properties of aerosols of anthropogenic origin plays a key role in improving their representation in atmospheric models and reducing uncertainties in climate and air quality assessments. This task aims to complement data collection and analysis from WP1 by utilising specific sensitivity simulations using state-of-the-art modelling frameworks from WP3 and WP4. Here, we work on constraining the chemistry, microphysics, and optical properties of anthropogenic aerosols, including their interactions with clouds. The introduction of methyl sulfonic acid, brown carbon and general model development in Earth system model simulations with OpenIFS and EC-Earth3 will feed into WP3 for further model improvement.

For the regional modelling, this task will employ the Weather and Research Forecast (WRF) and Multiscale Online Nonhydrostatic Atmosphere Chemistry (MONARCH) models to perform sensitivity simulations. With WRF, the impacts of initialisation and configuration on the simulations are analysed. For the MONARCH, simulation analyses aim at reducing uncertainties related to organic aerosols (OA), brown carbon (BrC) and their interactions with emissions and ageing processes. The ensemble of simulations will be evaluated against observational datasets from WP1 to ultimately contribute to a more robust representation of aerosol processes in WP4 and WP5.

In the following sections we will detail sensitivity simulations with OpenIFS, EC-Earth3 and its submodel TM5 with new developments in section 2. In section 3, the analysis of the initialisation and configuration simulations with WRF is presented. Section 4 describes the work on radiative properties of organic aerosols and BrC using the observations and MONARCH model. We summarise the work in section 5 and give a short outlook in section 6.

2. SENSITIVITY SIMULATIONS WITH OPENIFS/EC-EARTH3

In this section we detail climate model sensitivity simulations using EC-Earth3 and OpenIFS, with a focus on brown carbon (BrC), methyl sulfonic acid (MSA) and particle number concentrations. Brown carbon, a key component of atmospheric aerosols, has significant implications for climate forcing, air quality, and human health. In EC-Earth3 simulations, we explore the role of BrC for radiative balance of the atmosphere. Sensitivity simulations with methyl sulfonic acid (MSA) using EC-Earth3 provide new information on its effect on the cloud condensation nuclei concentrations. OpenIFS simulations of the aerosol model implementation in WP3 are analysed briefly here to provide next steps in the model development within the project. Furthermore, here we detail work towards providing a CCN climatology using machine learning methods to improve climate model simulations of cloud effects within the earth system.

2.1 Analysis of OpenIFS simulations

Within the WP3 of the FOCI project, the HAM-M7 (Hamburg Aerosol Model M7; Tegen et al. 2019, Vignati et al. 2004) has been implemented within the OpenIFS/AC (Open Integrated Forecasting System Atmospheric composition; Huijnen et al. 2022) model. The model simulates the aerosol population with 7 modes (4 soluble and 3 insoluble) representing sulphate, organic carbon, black carbon, dust and sea salt. Processes of aerosol nucleation, coagulation, condensation, sedimentation, dry and wet deposition are implemented. Here we summarise the results from two simulations to provide an initial evaluation into the performance of the model. We show here the results from earlier Cy43r3 and current Cy48r1 versions of the OpenIFS-HAM-M7

development work. The simulation done with OpenIFS-HAM-M7 Cy43r3 has one year of spin up and one year of analysed data for year 2010. This version uses the CMIP6 emissions as detailed in (Hoesly et al. 2018; van Marle et al. 2017). For the OpenIFS-HAM-M7 Cy48r1 we can at the moment utilise only the CAMS reanalysis emission data (https://atmosphere.copernicus.eu/sites/default/files/publications/CAMS261_2021SC1_D6.1.2-2022_202306_Docu_v1_APPROVED_Ver1.pdf; accessed 25.2.2025). This version has only one-month limited sensitivity simulation (July 2023) due to issues with continuing a run from restart files.

Table 2.1: Global aerosol budgets for sulphate (SO_4), organic aerosols (OA), black carbon (BC), sea salt (SS) and dust (DU) simulated for year 2010 using OpenIFS-HAM-M7 (base OpenIFS Cy43r3). For SO_4, there is no emission information as it is produced through oxidation.

	SO_4	OA	BC	SS	DU
Emission (Tg / year)		102.1	9.20	1940.3	1407.7
Total removal (Tg / year)	84.6	102.8	9.26	1939.6	1409.2
Wet deposition (Tg / year)	76.3	83.3	7.46	995.0	55.6
Dry deposition (Tg / year)	6.56	18.8	1.73	161.7	510.4
Sedimentation (Tg / year)	1.78	0.70	0.07	782.9	843.2
Burden (Tg)	3.60	6.14	0.53	10.6	2.64

The first evaluation of OpenIFS-HAM-M7 Cy43r3 shows that the production and removal processes of aerosols match each other in magnitude globally (see Table. 2.1). Compared to the literature estimates, the burdens are 2-4 times higher for sulphate, OA and BC compared to that from model median in AeroCom Phase3 comparison (Gliss et al. 2021). Furthermore, for example the burden of BC is roughly 4 times higher than that in Mann et al. (2010) while emission is only 20% higher. The larger burden is mainly caused by a known issue in wet removal scheme where convective fluxes are incorrect. The correction is already implemented in the OpenIFS Cy48r1 in WP3. Even with the shortcomings in the model parameterisation, wet deposition fractions of OA, BC and sulphate are similar to modal GLOMAP-mode model in Mann et al. (2010) with 81%, 81% and 90% fractions (Mann et al: 85%, 80%, and 90%), respectively. The sea salt emissions are low in our evaluation runs while dust emission is almost the same as median model in Gliss et al (2021). Despite rather similar emissions of dust, the burden is 6 times lower compared to their median model. A more comprehensive evaluation of global aerosol budgets will be done in WP3.

The simulated aerosol optical depth (AOD) for 2010 in OpenIFS-HAM-M7 Cy43r3 is 0.28 while the MODIS retrieval shows only 0.17 (see Figure 2.1). As noted earlier, this is caused by shortcomings in the parameterisation of wet removal in convective precipitation. This has been fixed in the later Cy48r1 and seems to be correcting the issue, however, a separate examination outside timeline of this WP is needed. In general, the simulated AOD is overestimated across the globe, whilst the dust emission regions seem to have lower AOD in the simulation (e.g. Sahara) and biomass burning regions in the Tropics (Africa and South America) exhibit higher AOD. For the OpenIFS CY48r1, the evaluation of AOD is not meaningful without a spin up period.

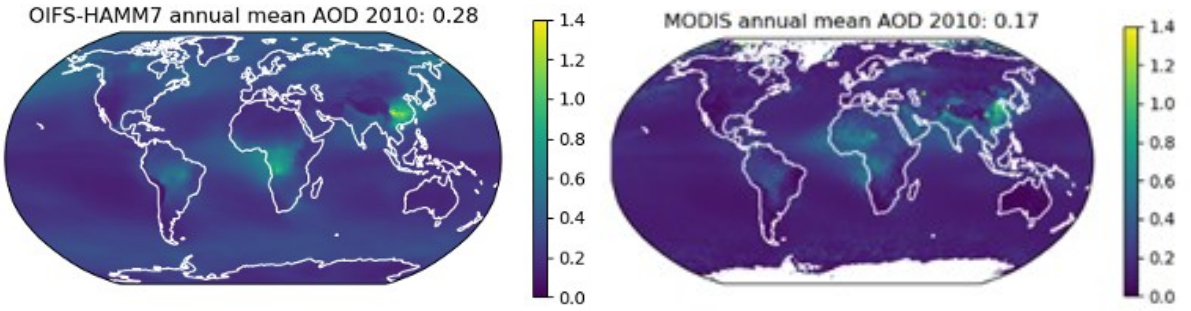

Figure 2.1: Annual mean aerosol optical depth for year 2010 simulated using OpenIFS (left) and from MODIS satellite retrieval (right).

As an initial evaluation of the particle number concentrations in OpenIFS-HAM-M7 Cy48r1, we show in Figure 2.2 a comparison of one month of number concentration data for July 2023 between ACTRIS (Aerosol, Clouds and Trace Gases Research Infrastructure; Laj et al. 2024) station observations and model. The model shows mainly underestimation of the concentrations compared to observations with high aerosol loading. This simulation lacks new particle formation (NPF) and proper spin up. Therefore, we expect higher concentrations from the simulations with updated model version and spin up; this preliminary sensitivity run gives some confidence that the consistent implementation of aerosols is nearing its completion. However, the model evaluation needs a full year of simulation with proper spin up to allow the aerosol fields to develop. Unfortunately, the OpenIFS Cy48r1 version needs more development work on NPF and wet scavenging in convective clouds. Furthermore, the restarting capability is limiting options as running two years in one go is not feasible due to time needed for the computations.

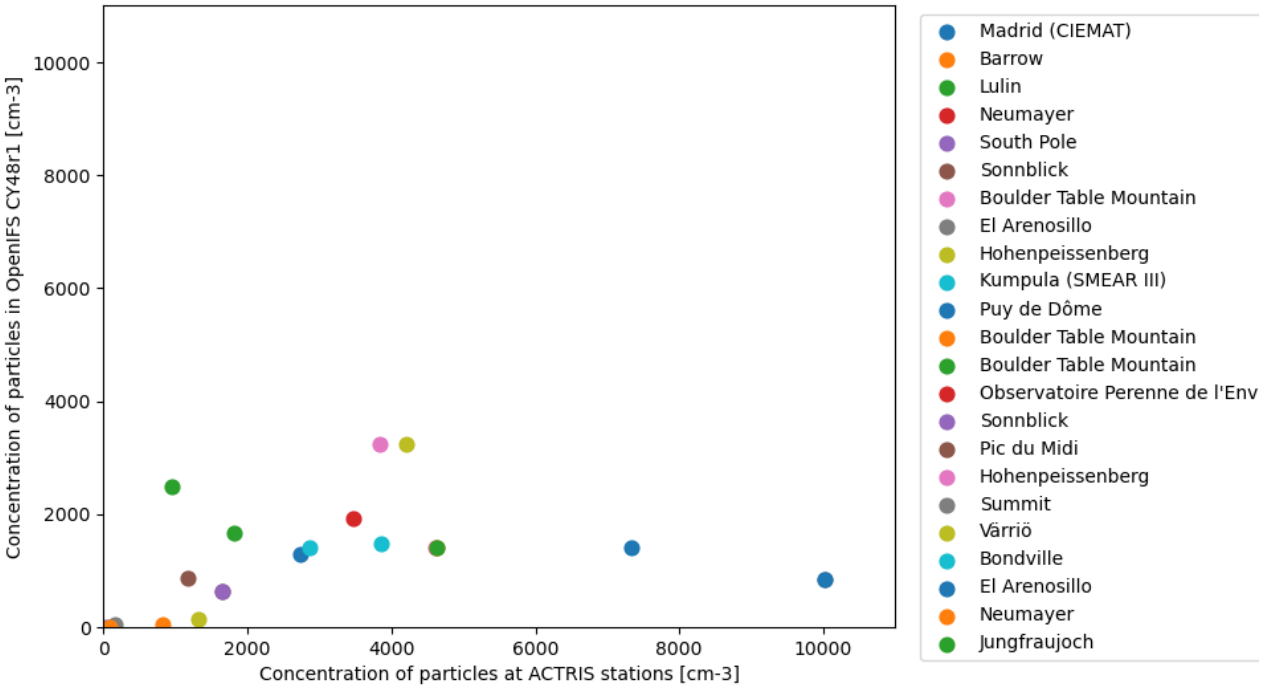

Figure 2.2: Scatter plot of simulated and observed aerosol number concentration at ACTRIS stations.

2.2 Observation-based cloud droplet climatology

In the Cy43r3 version of OpenIFS the cloud droplet (CD) number concentrations are represented with two constant values, one for continents and one for oceans. Since the real CD concentration is heavily dependent on cloud condensation nuclei (CCN) concentration, which, in turn is affected by several primary particle and secondary aerosol sources, this simplification is obviously making the OpenIFS clouds unsensitive to any aerosol processes. We have started the process of implementing in OpenIFS global observation-based CD climatologies based on 35 long-term data sets of particle number size distribution data around the world, CAMS re-analysis data and machine learning (ML) models (Ovaska et al., *in preparation*). The ML models (multi-linear regression model and XGBoost model) utilise global continental observations of daily number concentrations of particles larger than 100 nm in diameter (N100), serving as approximations for CCN, as the target variable and CAMS re-analysis data on gas and aerosol concentrations and meteorology as predictor variables. Based on our cross-validation results, the ML model performance is good in environments that are well represented in the training data, with 70% of daily N100 concentrations reproduced within a factor of 1.5 from the observed concentration. However, in the environments that are not well represented, the results are the less reliable the more the environment diverges from those represented well (Figs. 2.3 and 2.4).

The output of the ML models, time series of daily N100 concentrations with the CAMS spatial resolution for 20 years (2000–2020), will be converted to monthly CD concentration climatologies with simple CCN-to-CD parameterisations (e.g., Gultepe and Isaac, 1999), and finally these climatologies will be implemented in the OpenIFS.

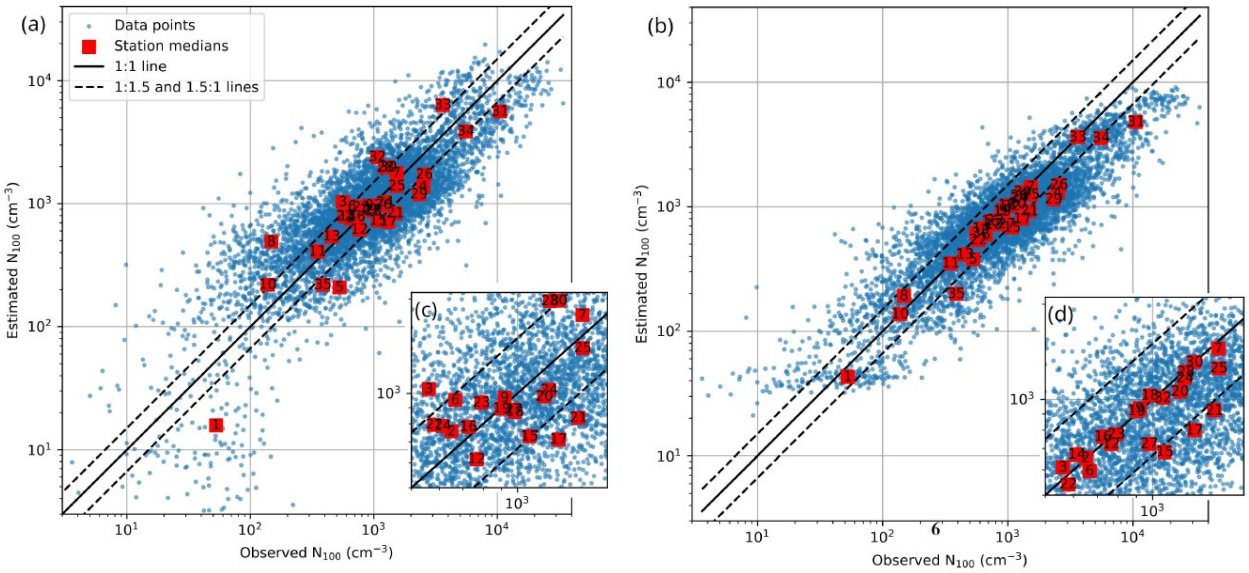

Figure 2.3: Comparison between observed and estimated number concentration of particles with diameter larger than 100 nm (N100). Panel a) shows the result for station-excluded multi-linear regression models and panel c) shows a zoom-in. Panels b) and d) show the result and zoom-in for station-excluded XG Boost models, respectively. The daily values are indicated in blue and station medians in red. The dashed lines show the deviation by factor 1.5 from the observations, which Rosenfeld et al. (2014) estimated as the required accuracy for CCN concentrations for reliably assessing aerosol effects on clouds.

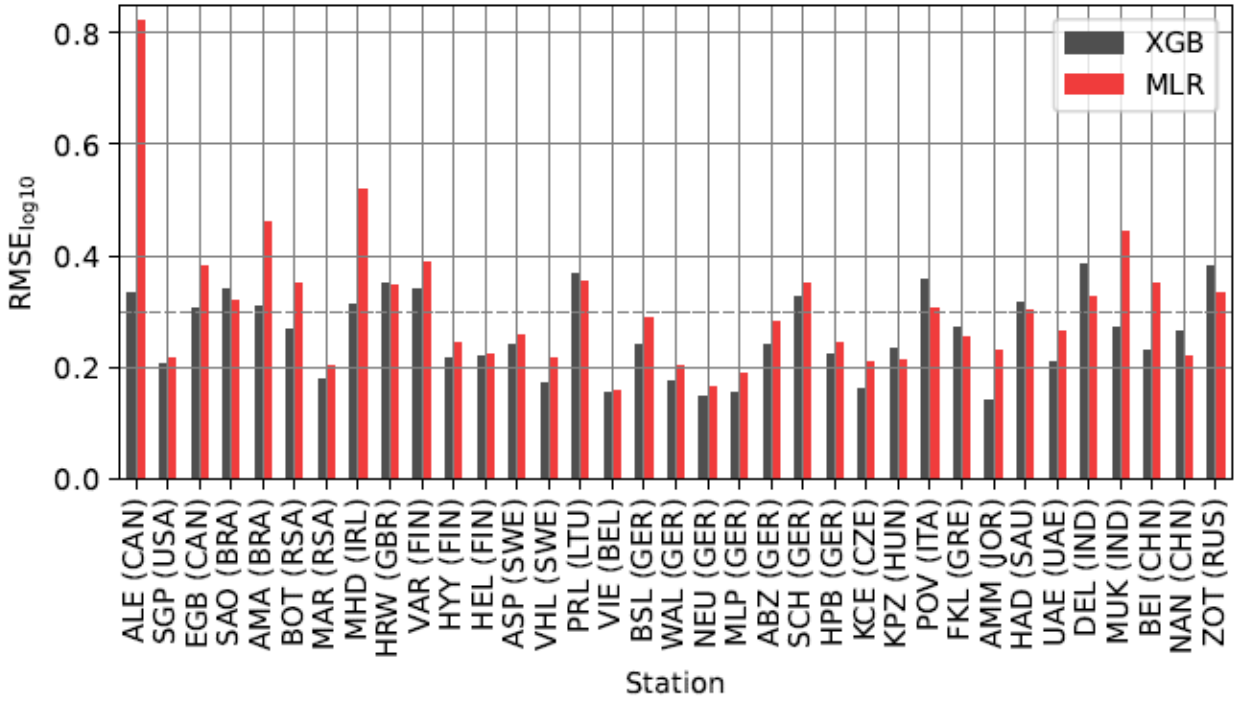

Figure 2.4. Comparison between station-excluded multi-linear regression (MLR) and XG Boost (XGB) model performance expressed as RMSE between daily estimates and observations, calculated for log10-transformed concentrations at each station. RMSE values 0.2 and 0.3 correspond to roughly 70% and 50%, respectively, of estimated daily concentrations being within a factor 1.5 of the observed concentrations (i.e., between 0.67×observation and 1.5×observation), which Rosenfeld et al. (2014) estimated as the required accuracy for CCN concentrations for reliably assessing aerosol effects on clouds.

2.3 Sensitivity runs on partitioning of MSA in EC-Earth3

In EC-Earth3/TM5, MSA is produced from DMS via the OH oxidation pathway (Huijnen et al., 2010). A bug in TM5 caused EC-Earth3-CMIP6 simulations to completely omit MSA-derived aerosols. After a bug-fix, EC-Earth3 treats MSA as bulk aerosol that is assumed to condense only in the accumulation mode without effect on nucleation processes or on the early growth of nanometer-sized particles. FMI has developed the MSA treatment to also represent the potential effect of MSA on smaller particles (Hodshire et al., 2019). New developments and evaluation have been performed with TM5 and will be transferred to OpenIFS/EC-Earth4. In the new methodology, MSA is treated as a mixture of Extremely Low Volatility Organic Compounds (ELVOC) and Semi-Volatile Organic Compounds (SVOC), according to the scheme by Bergman et al. (2022). This allows us to assess its importance for aerosol nucleation and growth, as well as condensation to the whole aerosol population. Figure 2.5 shows impact of MSA volatility assumption on CCN, quantified as a difference in CCN concentration (at 0.2% supersaturation) between simulations with MSA as purely ELVOC compared to simulation with ELVOC as SVOC.

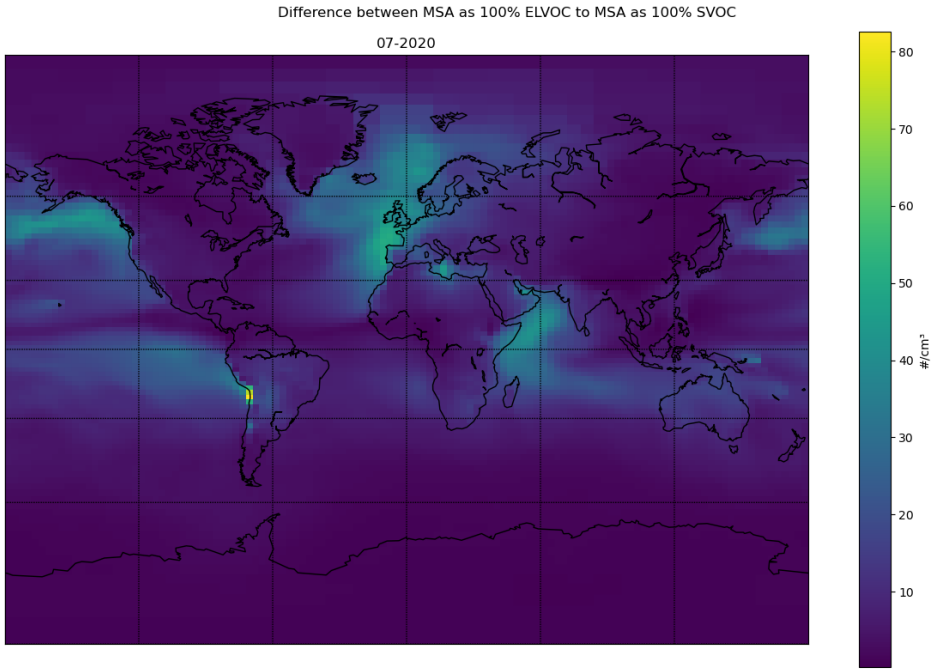

Figure 2.5: Impact of MSA on CCN at 0.2% supersaturation (see details in the text).

2.4 Updated BrC emissions in EC-Earth3

We have investigated the global radiative impacts of anthropogenic Brown Carbon (BrC) emissions using the EC-Earth3 Earth System Model. The aim was to advance the representation of BrC within climate models by integrating additional emission sources to improve the accuracy of its radiative effect estimates. Additionally, we explored the role of BrC in driving regional climate variability and its broader contribution to global climate forcing. BrC emissions were prepared by the Finnish Environment Institute for IIASA's ECLIPSE dataset (Evaluating the Climate and Air Quality Impacts of Short-lived Pollutants; Stohl et al., 2015), which also provide data on Organic Carbon (OC) and Black Carbon (BC) emissions.

The format of the emission data was transferred to match the input format of the EC-Earth3 (model version: r9695-forces-brown-carbon). This update replaced portions of OC, BC, and BrC emissions with new data. In control simulations, we replaced original OC and BC emissions with ECLIPSE data and afterwards anthropogenic BrC were added to the simulations (BrC_{anth}). Identical OC and BC emissions were used in the control and BrC_{anth} simulation. We applied the biomass and biofuel burning parameterization for anthropogenic BrC from Saleh et al. (2014), which defines emitted BrC absorption as a function of the BC/OA (organic aerosol) emission ratio. The simulations were conducted across several periods (1990, 2010, 2020 and 2040) to represent both historical and future scenarios. Each simulation ran for six years, including a one-year spin-up period. The FIXYEAR configuration in EC-Earth3 (fix emissions to a given year) was used to minimize variability and enhance the comparability of the simulation outputs. The simulated BrC burdens for the two simulations are listed in Table 2.2. The refractive indices used for different aerosol species are given in Table 2.3.

Table 2.2: Global averages of BrC burden for simulations with and without anthropogenic BrC sources in 1990 and 2010.

	BrC burden (Tg)	
Year	without anthropogenic sources	with anthropogenic sources
1990	1.357×10^{-1}	9.071×10^{-2}
2010	1.524×10^{-1}	1.071×10^{-1}
2020	1.362×10^{-1}	9.604×10^{-2}
2040	1.323×10^{-1}	9.597×10^{-2}

The total BrC emissions are divided into partly inert BrC (6%) and reactive BrC (94%) in the EC-Earth3. Also, photobleached BrC in the model were calculated using observed bleaching rate with a mean value of 0.24 ± 0.10 day^{-1} (Fang et al., 2023).

Table 2.3: Radiative refractive indices of black carbon (BC), organic carbon (OC), reactive brown carbon (rBrC), inert brown carbon (iBrC) and photobleached brown carbon (pbBrC) for three wavelengths.

Wavelength	BC (Real + Img)	OC (Real + Img)	rBrC (Real + Img)	iBrC (Real + Img)	pbBrC (Real + Img)
~300 nm	1.83985 + 0.75809i	1.53000 + 0.00000i	1.00000 + 1.16918i	1.00000 + 0.34721i	1.00000 + 0.75286i
~500 nm	1.85000 + 0.70516i	1.53000 + 0.00000i	1.00000 + 0.04542i	1.00000 + 0.04930i	1.00000 + 0.00804i
~600 nm	1.85000 + 0.70193i	1.53000 + 0.00000i	1.00000 + 0.03422i	1.00000 + 0.04187i	1.00000 + 0.00532i

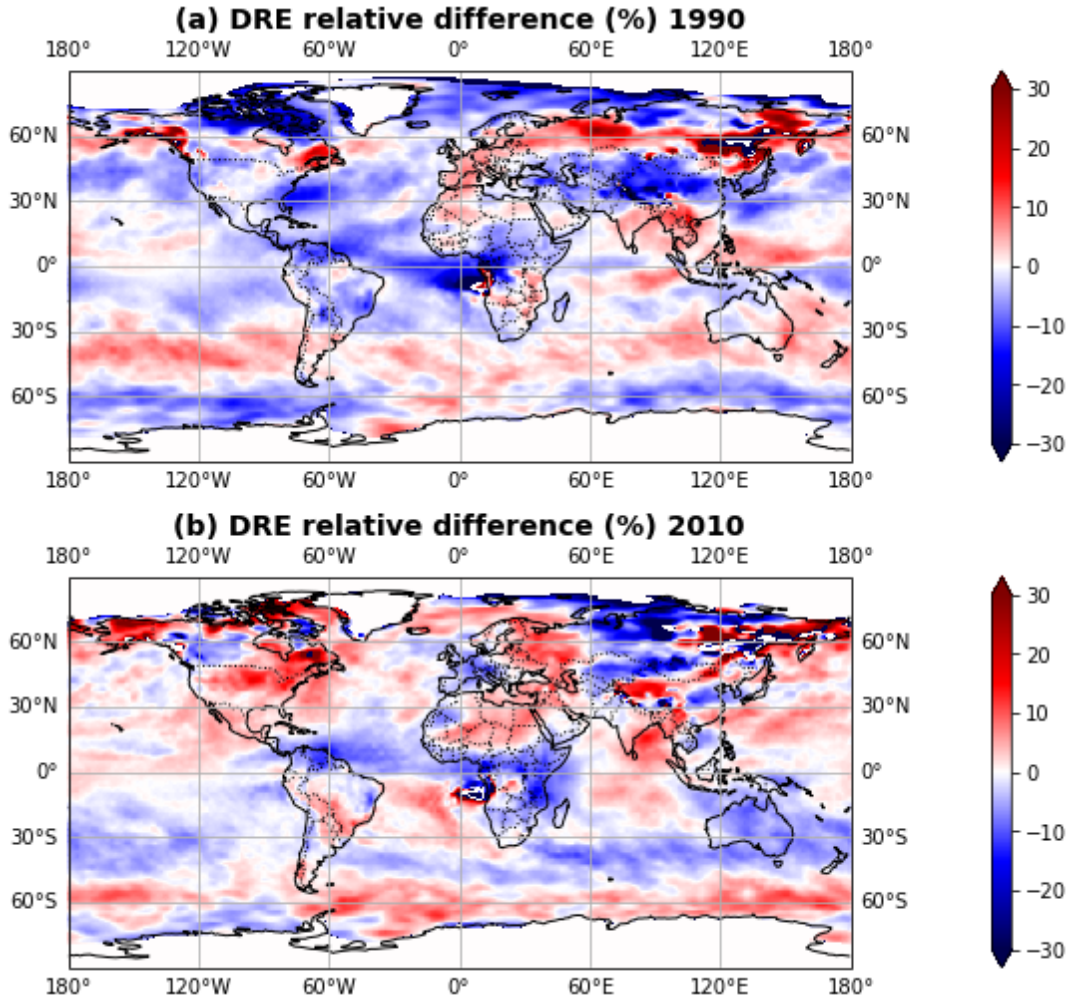

Figure 2.6: Relative difference (%) of direct radiative effect (DRE) between the control and anthropogenic BrC simulations for (a) 1990 and (b) 2020. (Relative Difference = (control – BrCanth) / control × 100), here 'BrCanth' is the simulation with anthropogenic BrC, and 'control' is the control simulation of EC-Earth).

Figure 2.6 presents the relative impact of anthropogenic BrC based on the historical simulations for the years 1990 and 2010. As the figures show, the global mean impact of anthropogenic BrC emissions on DRE is negligible. However, in both periods, the DRE over the tropical regions of Africa and the eastern part of China is significantly more pronounced due to anthropogenic BrC. The global averages of DRE due to anthropogenic BrC are about 0.025 and 0.004 Wm^{-2} in 1990 and 2010, respectively.

3. SENSITIVITY SIMULATIONS USING WRF

The performance of the Weather Research and Forecast (WRF) model depends on many environmental factors such as land use and land cover (LULC) characteristics, meteorological fields as the initial and forcing boundary conditions (ICBC) data, and various model physics scheme configuration. Nine sensitivity simulations were performed using WRF model over the EURO-CORDEX domain (195×195 grid points and grid spacing of 27 km) in 2018 to assess the WRF performance under different configurations and input datasets. The results of

these runs will be used to confirm a benchmark for the long-term climatic simulations in the FOCI project (https://www.project-foci.eu/wp/).

Meteorological fields are important as they are used as input for the atmospheric chemistry modelling systems. Therefore, the suggestion of the best WRF configuration to achieve reliable simulation of temperature, radiation, humidity, wind field, and planetary boundary layer height (PBLH), which directly affect the concentration of chemical parameters (e.g. ozone and aerosol) concentrations, is necessary.

The main purposes of the sensitivity simulations are listed below:

1. Sensitivity of WRF to two LULC datasets (MODIS IGBP and "Land Use and Climate Across Scales" (LUCAS)
   As future simulations under different SSPs and RCPs pathways are needed in the FOCI project, LUCAS future projection dataset (Hoffmann et al., 2022a) has been selected as LULC input data. To follow a consistent method, LUCAS data from historical period (Hoffmann et al., 2022b) will be used in the FOCI historical simulations. Therefore, the WRF sensitivity to high-resolution LUCAS dataset is compared with the default MODIS IGBP LULC.
2. Sensitivity of WRF to two ICBC datasets (NCEP Final Operational Global Analysis (NCEP-FNL) and ECMWF (the European Centre for Medium-Range Weather Forecasting) Reanalysis v5.0 (ERA5; Herschbach et al. 2020))
   It is expected that applying *reanalysis* datasets such as ERA5 improves the quality of the numerical results in comparison to the *analysis* datasets such as NCEP-FNL (National Centers for Environmental Prediction, 2000), because *reanalysis* data include observations that were not available at the time of the global simulations (Parker, 2016; Parra, 2022). However, in some regions, using NCEP-FNL datasets shows better results than ERA5 in simulation of temperature and wind speed (Parra, 2022). The reliability of the two ICBC datasets in the European domain in estimation of near surface meteorological fields will be assessed.
3. Sensitivity of WRF to two nudging techniques
   Two nudging options in the WRF, including grid-nudging and spectral nudging, are assessed, as the nudging technique can overcome the deviation from the driving fields in high-resolution simulations caused by dynamical downscaling. From the literature review, the performance of the WRF model using nudging options changes regionally. Proper nudging option can improve the numerical results reliability in the simulation of the temperature, wind fields, precipitation, and PBLH, which will be used as an input for the atmospheric chemistry models (Jeon et al., 2015; Ho et al., 2024).
4. Sensitivity of WRF to initialization method
   In the daily-initialization method, each run starts from 12:00 UTC of the day before the target day, which is considered as 12 hours spin-up, and contains 36 hours of WRF output. Each daily simulation is independent from the other days, which is an advantage of performing parallel runs. This method avoids a significant deviation from the ICBC forcing data, which is the main purpose of using this approach. Results from this simulation (S1a) will be compared to a continuous run with two-weeks spin-up (S1b), with similar model configurations and input ICBC and LULC datasets.
5. Sensitivity of WRF to model configuration
   Different combinations of microphysics, surface layer, boundary layer and cumulus parameterization schemes are assessed. The literature review shows that the local and regional performance of WRF depends on the proper selection of the physical parametrization schemes (Santos-Alamillos et al., 2013; Stergiou et al., 2017).

3.1 Observations

Global hourly INTEGRATED SURFACE DATA (ISD) observations for near-surface air temperature (T2m) from National Oceanic and Atmospheric Administration (NOAA) (available from: https://www.ncei.noaa.gov/data/global-hourly/access/) for 115 urban-background stations (airports) in the Europe domain have been used for model evaluation. The general performance of the WRF model is evaluated with the use of following metrics:

FAC2:	the fraction of predictions within a factor of two of observation,
MB:	Mean bias, MGE: Mean gross error,
NMB:	Normalized mean bias,
NMGE:	Normalized mean gross error,
RMSE:	Root mean squared error,
r:	Correlation coefficient,
r^2:	Pearson coefficient,
P:	A p-value which is a statistical measurement used to validate a hypothesis against observed data,
COE:	Coefficient of efficiency and IOA: Index of agreement.

3.2 Results of the sensitivity analyses for T2m over Europe

Temperature is one of the critical parameters for atmospheric chemistry and urban air quality as it affects the structure of the planetary boundary layer (Du et al., 2020) and chemical reactions in the atmosphere (Coates et al., 2016). Temperature directly affects the VOCs emission from natural and anthropogenic sources (EPA, 2025; Debevec et al., 2021) which influences ozone and aerosol formation (Gupta et al, 2024; Payra et al., 2022).

From the first analysis of the numerical results, significant bias from the observation was observed in T2m estimation in the coastal stations. To improve the results in these areas, in the final sensitivity run (S6) the impact of using skin-temperature instead of surface sea temperature in the forcing ERA5 ICBC dataset on model performance is explored.

Figure 3.1 shows the annual mean T2m bias (model-observation) in 115 stations over Europe domain, which shows better performance of the WRF model in the central and northern Europe than southern Europe. The highest bias between model and simulation is observed in the western coastal areas of Italy. In addition, S1a and S6 configurations improves the results in the UK, and central and northern Europe. Table A1 shows the calculated statistical metrics of T2m annual averages over all selected stations. Extremes values from observations are compared with the numerical results in Table A2.

The primary analysis of numerical results shows that model configurations applied in S1a and S6 show the highest accuracy on T2m simulation. As the main purpose of the sensitivity experiments is suggestion of the best configuration for the long-term climate-scale runs, the daily-initialization method used in S1a is not applicable. Therefore, S6 configuration is the final suggestion for the Europe domain. However, further model evaluation for wind speed, relative humidity and PBLH are needed.

Table 3.1. WRF configuration and sensitivity simulations (C3R-UH)

Sensitivity Simulation	ICBC	LULC	Microphysics Option	Surface Layer	Boundary layer (PBL)	Cumulus parameterization	Nudging technique[5]
S1a[1]	NCEP-FNL	MODIS IGBP	Morrison 2-mom[3]	Revised MM5 Monin-Obukhov	Yonsei University (YSU)	Grell-Freitas ensemble	GN
S1b	NCEP-FNL	MODIS IGBP	Morrison 2-mom	Revised MM5 Monin-Obukhov	YSU	Grell-Freitas ensemble	GN
S2	ERA5	MODIS IGBP	Morrison 2-mom	Revised MM5 Monin-Obukhov	YSU	Grell-Freitas ensemble	GN
S3	NCEP-FNL	LUCAS	Morrison 2-mom	Revised MM5 Monin-Obukhov	YSU	Grell-Freitas ensemble	GN
S4a	ERA5	LUCAS	Morrison 2-mom	Revised MM5 Monin-Obukhov	YSU	Grell-Freitas ensemble	GN
S4b	ERA5	LUCAS	Morrison 2-mom	Revised MM5 Monin-Obukhov	YSU	Grell-Freitas ensemble	SN
S5a	ERA5	LUCAS	Thompson[4]	MYNN surface layer	MYNN 2.5 level TKE	Kain-Fritsch (new Eta)	GN
S5b	ERA5	LUCAS	Thompson	MYNN surface layer	MYNN 2.5 level TKE	Kain-Fritsch (new Eta)	SN
S6[2]	ERA5	LUCAS	Morrison 2-mom	MYNN surface layer	MYNN 2.5 level TKE	Grell-Freitas ensemble	SN

[1] Daily initialization method
[2] Skin Temperature is considered instead of Sea Surface Temperature in ICBC input data.
[3] Morrison double-moment scheme. Double-moment ice, snow, rain and graupel for cloud-resolving simulations.
[4] Thompson scheme: A scheme with ice, snow and graupel processes suitable for high-resolution simulations.
[5] Grid-Nudging (GN); Spectral Nudging (SN)
Applied in all simulations:
Radiation: Longwave RRTMG scheme and RRTMG shortwave scheme (Iacono et al., 2008), and Land-surface model: Unified Noah land-surface (Tewari et al., 2004).

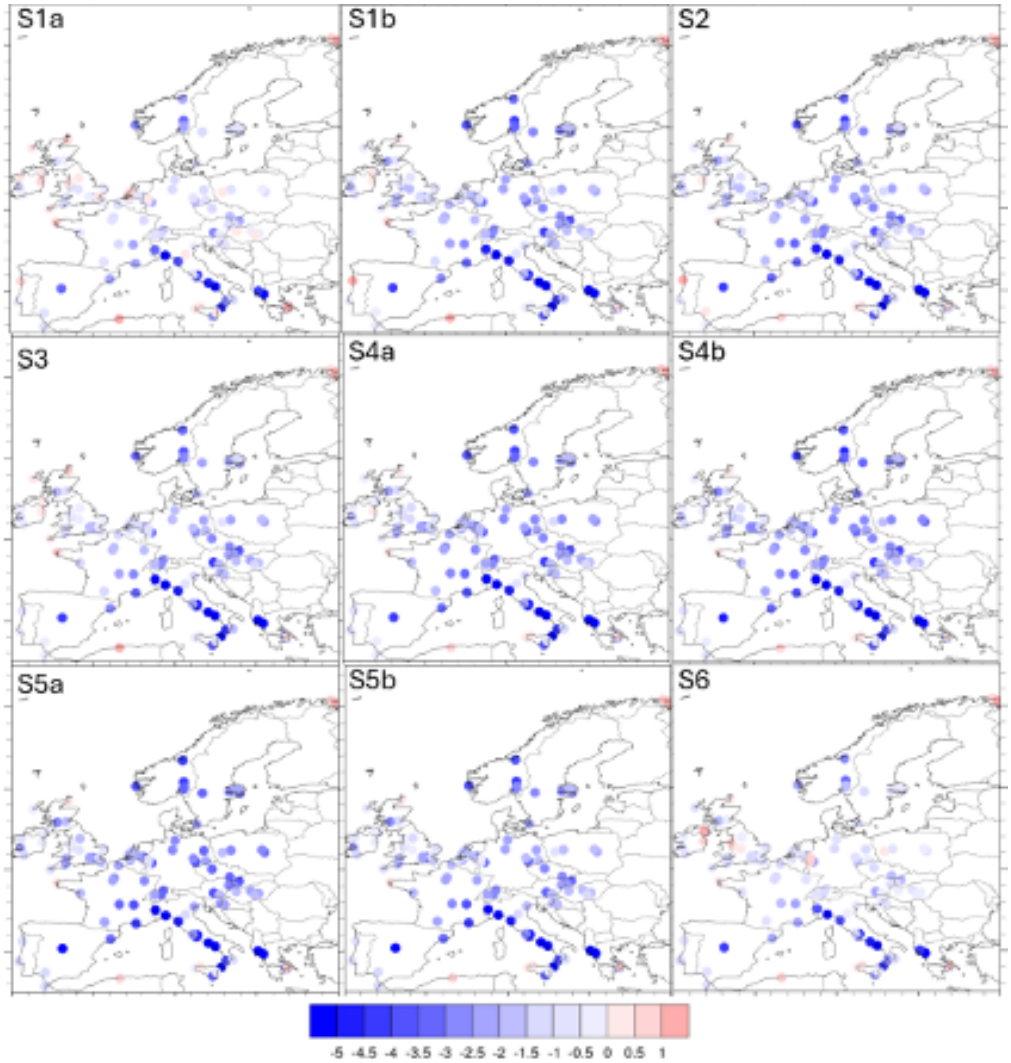

Figure 3.1: Annual mean 2m air temperature bias (model-observation) in 115 stations over Europe domain.

4. INVESTIGATING ORGANIC AEROSOL ABSORPTION PROPERTIES AND BrC REPRESENTATION IN MODELS

This section presents two modelling studies investigating the absorbing properties of organic aerosols (OA). First, we investigate the light absorption properties of OA at different environments across Europe combining both modelling techniques and experimental approaches to constrain specific imaginary refractive indexes (k) for OA originating from different emission sources. Second, we analyze the intra-annual variability of brown carbon (BrC) simulated by a scheme accounting for primary biomass burning (BB) and biofuel (BF) BrC sources that undergoes photobleaching effects. Sensitivity runs perturbing BrC emissions are analyzed to investigate the uncertainties in the emission sources.

4.1 Characterization of organic aerosol imaginary refractive index

Brown carbon (BrC) is a subset of organic aerosols (OA) that significantly absorbs light in the near-ultraviolet (UV) and visible regions of the spectrum. Unlike black carbon (BC), which primarily originates from the

incomplete combustion of fossil fuels and biomass, BrC is produced from a variety of sources, including biomass burning (BB), biofuel (BF), fuel combustion, and SOA formation (Laskin et al. 2015, Saleh et al. 2014). BrC has gained increasing attention in recent years due to its potential impact on climate (Li et al. 2023). The absorption characteristics of BrC remain insufficiently constrained, with studies indicating that the imaginary refractive index of BrC can vary by 30-50% (Wang et al. 2013). This range of variability is attributed to emission sources and the physicochemical composition of BrC molecules.

Here, we aim to derive representative imaginary refractive indexes for OA originating from different emission sources, such as fires, residential, shipping, traffic, and others. We use the Multiscale Online Nonhydrostatic Atmosphere Chemistry model (MONARCH; Badia et al., 2017; Navarro-Barboza et al., 2024) to simulate the light absorption of OA in Europe during 2018. The results provide an estimate of OA light absorbing properties in Europe as an attempt to constrain OA optical properties representative of field conditions based on the current knowledge on emission sources and transport modelling. This work has been published in Navarro-Barboza et al. (2025).

4.1.1 Observational dataset and modelling setup

The OA/Organic Carbon (OC) mass concentrations and multi-wavelengths absorption measurements used in this study were collected at 12 sites in Europe covering urban, suburban, and regional background environments. The dataset was prepared in Task 1.2 of WP1. Figure 4.1 show the geographical locations of the stations and the relative contribution of black carbon (BC) and BrC to the total absorption measured at 370 nm. The contribution of BrC ($b_{abs,BrC}$ (λ)) to the total measured absorption ($b_{abs}(\lambda)$) at different wavelengths from 370 nm to 660 nm was estimated by subtracting the absorption due to BC ($b_{abs,BC}(\lambda)$ to the measured ($b_{abs}(\lambda)$):

$$b_{abs,BC}(\lambda) = b_{abs}(880\ nm) \cdot (\lambda/880\ nm)^{-AAE\_BC}$$

$$b_{abs,BrC}(\lambda) = b_{abs}(\lambda) - b_{abs,BC}(\lambda)$$

where AAE_BC is the Absorption Angstrom Exponent (AAE) of BC, which allows for the calculation of $b_{abs,BC}(\lambda)$ (in units of Mm−1) from the measurements of $b_{abs,BC}(\lambda)$ at 880 nm assuming that BrC does not absorb at 880 nm (e.g., Qin et al., 2018).

In this work, we use the BrC absorption at 370 nm given that the BrC absorption efficiency is the highest in the UV spectral range, and consequently, the observed BrC absorption is less uncertain compared to the visible range. A low BrC contribution, around 14%, was observed at the urban sites of BCN and HEL, both affected by direct traffic emissions, making BC the dominant absorber at these sites. MAR urban site registered higher BrC contribution (30%) likely reflecting the accumulation of biomass burning emissions in winter and the presence of BrC sources as shipping emissions. Suburban stations, including SIR, KRA, and DEM, exhibit BrC contributions from 22% to 30%, reflecting a blend of local urban emissions and regional influences such as biomass burning and coal combustion. KRA is considered a pollution hotspot in Europe (e.g. Casotto et al., 2023) with high consumption of coal and wood (both important sources of BrC) for energy production and residential heating, making the OA concentrations measured in KRA the highest among the European measuring sites. DEM and SIR are affected by biomass burning emissions especially in winter, which causes a considerable accumulation of BrC during the cold season. Regional stations, represented by HYY, OPE, RIG, PAY, IPR, and MSY, present BrC contributions from 21% to 41%. These percentages indicate a mixture of biogenic sources, local emissions, agricultural activities, and transboundary pollution that affects the regional

atmosphere. IPR stands out with the highest contribution (around 40%), suggesting a significant contribution of low-temperature combustion processes as residential sources. Overall, although BC typically represents the most absorbing aerosols component at these stations (usually > 70%), it is noteworthy that BrC could contribute comparably to absorption in some instances.

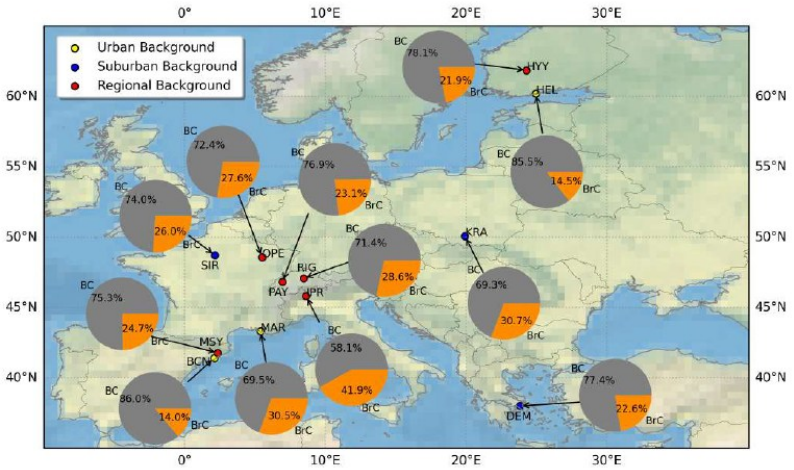

Figure 4.1: Annual average contributions [%] of BrC (orange) and BC (gray) to the total absorption at 370 nm measured at 12 monitoring stations across Europe in 2018. Source: Navarro-Barboza et al. (2025)

The MONARCH atmospheric chemistry model is used to simulate the OA mass over Europe and their source contribution. MONARCH is an online integrated system for meso-scale to global-scale applications with telescoping nesting capabilities. MONARCH relies on the CB05 chemical mechanism extended with chlorine chemistry. A simplified gas–aqueous–aerosol mechanism accounts for sulfur chemistry (Spada, 2015) and the EQSAM thermodynamic equilibrium module for the production of secondary nitrate–ammonium aerosol. The simple scheme proposed by Pai et al. (2020) is used for the formation of secondary organic aerosols. While a sectional approach is used for dust and sea salt, a bulk description of the other aerosol species is adopted. Meteorology-driven emissions are computed within MONARCH. Mineral dust emissions can be calculated using one of the schemes described in Klose et al. (2021), several source functions are available to compute sea salt aerosol emissions (Spada et al., 2013), while biogenic Non-Methane Volatile Organic Compounds (NMVOC) and soil NO emissions are estimated with the Model of Emissions of Gases and Aerosols from Nature (MEGAN) v2.04 model (Guenther et al., 2006).

The model is configured on a European domain at a horizontal resolution of 20 km. Anthropogenic emissions are provided by the European-scale emission inventory CAMS-REG-AP_v4.2 (Kuenen et al., 2022), while biomass burning (BB) emissions are derived from the Global Fire Assimilation System version 1.2 (GFASv1.2) analysis. This dataset provides detailed emission fluxes derived from satellite information for various sources such as forest, grassland, and agricultural waste fires (Kaiser et al., 2012). Additionally, for oceanic dimethyl sulfide (DMS) emissions, we relied on the CAMS Global Ocean dataset (Granier et al., 2019).

Perturbation runs (commonly known as the brute force method) were conducted to apportion the contribution from fires, traffic, shipping, residential, and other sources to OA concentrations. Biomass burning emissions derived from the GFASv1.2 product are tagged as GFAS. Traffic emissions (TRAF) categorized under sectors GNFR_F1, F2, F3, and F4 account for exhaust and non-exhaust emissions of gasoline, diesel and liquefied petroleum gas vehicles. Shipping emissions (SHIP) are derived from GNFR_D sector. The emissions from commercial, institutional and residential sources (RESI) consider a wide range of sources related to buildings

and facilities and are categorized under sector GNFR_C. RESI includes activities of combustion in different types of devices, including boilers, turbines, engines, and chimneys, for different fuel types (i.e., natural gas, wood, fuel oil, LPG, coal). In this sector, only combustion activities related to space heating, cooking, and water heating are included (cleaning activities are not considered). Furthermore, the rest of sources are tagged together as other sources (OTHR) including public power, industry, fugitives, solvents, aviation, off-road, waste, agriculture, and biogenic emissions.

We use an offline optical package (Obiso, 2018) to calculate the absorption by OA using the mass concentration simulated by the model. The package allows calculating intensive optical properties of a size-distributed particle ensemble, including the absorption efficiency (Qa) as the difference between extinction and scattering efficiencies. The real (n) and imaginary (k) parts of the complex refractive index determine the scattering and absorption properties of the particles, respectively, and primarily depend on their internal composition. The package is built on a data set of monodisperse single-wavelength optical properties, pre-calculated using the Mie-theory code by Mishchenko et al. (2002), whose structure allows computational efficiency while preserving application flexibility. Once obtained the size-integrated absorption efficiency, the absorption coefficient of OA is calculated.

Since k is a highly uncertain parameter with a strong dependence on the sources of OA, we employed a method to derive an optimized k for each OA component (aggregating both primary and secondary contribution) that combines the results of the perturbation runs, which provides source apportionment of OA mass, and observations shown in Figure 4.1. Based on the aerosol mass calculated by the model, we use the offline optical tool to derive k values that minimize the error with the absorption measured at the 12 monitoring stations across Europe (Figure 4.2 illustrates the steps of the optimization process). The optimized k values are derived using the SLSQP algorithm (Sequential Least Squares Programming), which is particularly well-suited for nonlinear objective functions and constraints to minimize a cost function. This process handles the task of minimizing the error between the modelled and the observed absorption. The cost function calculated here evaluates this error at each time step, guided by predefined bounds for k values derived from Saleh (2020). These conditions categorize OA absorption into four optical classes: very weakly absorptive OA (VW-OA), weakly absorptive OA (W-OA), moderately absorptive OA (M-OA), and strongly absorptive OA (S-OA). Note that Saleh (2020) categories for OA absorption were derived from 20 chamber experiments that may not be completely representative of ambient conditions in the field. The resulting k values are representative of OA in environmental conditions, which may include interactions with other species, providing an empirical range of k values that account for various OA sources and potential interference. To derive the absorption characteristics of different sources of OA, we conducted different optimization steps changing the boundaries where the optimized k value is allowed to vary until an optimal solution is obtained.

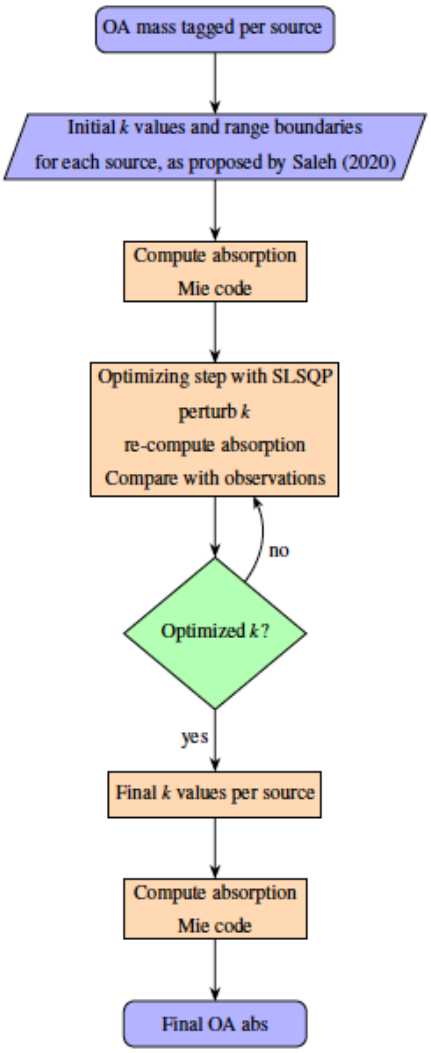

Figure 4.2: Steps to derive optimized k imaginary refractive index for OA. Source: Navarro-Barboza et al. (2025).

4.1.2 Results

This work focuses on understanding the light absorption properties of OA across different European environments. Since the light absorption of OA is intrinsically related to its mass concentration, the first step is to evaluate the accuracy and reliability of our model run in simulating mass concentrations. Figure 4.3 shows the time series of the measured and modelled OA mass concentrations for 2018 (note the varying y-axis scales in different panels). The modelled concentrations of OA, derived from the source-tagged simulation, are represented by filled colours, where each colour shows the contribution from different emission sources. Specifically, SHIP is marked in purple, RESI emissions in light blue, GFAS in orange, TRAF in black, and OTHR in brown (only primary contribution shown). Additionally, Secondary Organic Aerosols (SOA) contribution is depicted in green.

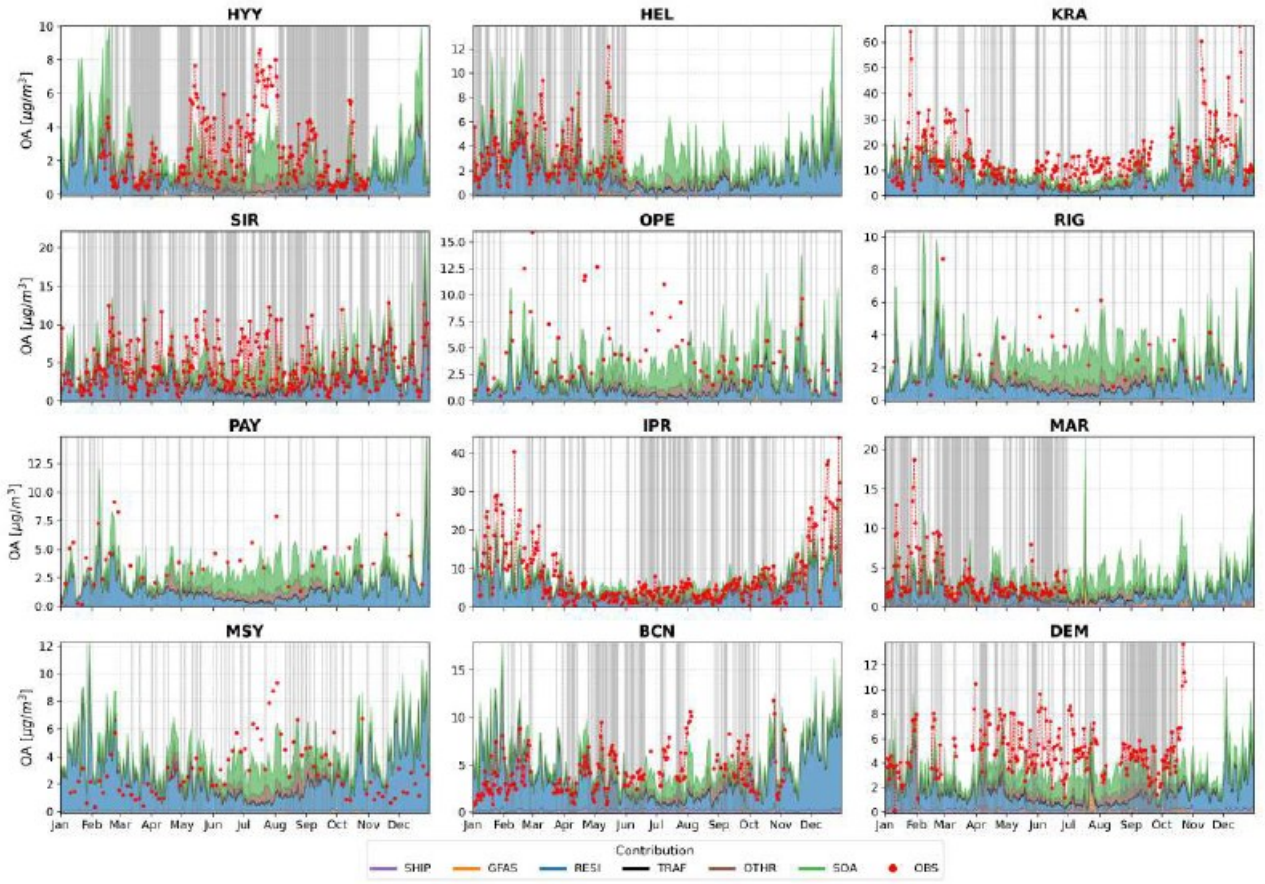

Figure 4.3: Observed and modelled daily mean OA mass concentrations and source contribution [μg m^{-3}]. Source: Navarro-Barboza et al. (2025).

MONARCH results showed good performance in simulating OA concentrations in most stations, meeting the evaluation statistical benchmarks throughout the year (see Navarro-Barboza et al. (2025) for further details), with peak performance in the spring season. RESI sources (which accounts for domestic heating, cooking, and water heating) dominated OA concentrations during the colder months. SOA emerged as the second most significant contributor, especially during warmer periods at regional sites, such as MSY, HYY, OPE, RIG, and PAY, though slightly underestimated in summer due to likely low biogenic SOA production in the model. SHIP emissions notably affected near-port stations, while TRAF emissions play a minor role. Despite the limitations identified, the model effectively captured specific events like wildfires and high-pollution episodes, demonstrating its ability to reproduce episodic events.

The optimization of the imaginary refractive index (k) at 370 nm for OA across the twelve measurement stations presented challenges, primarily due to limitations in data coverage. Data points for the optimization process were selected based on their consistency with observed OA concentrations. However, the availability of data varied significantly between stations, imposing limitations on the optimization process. The optimization process used a bias threshold selecting only days where the simulation fell within ±1.5 $\mu g m^{-3}$ of OA measurements (gray background in Figure 4.3). This approach aimed to improve the reliability of the results despite data limitations.

Optimizing by individual stations (stn) or by combining all data points (all) resulted in the k values summarized in Table 4.1. A robust estimation of GFAS k in-between weakly and moderately absorbing OA was found,

suggesting that GFAS OA cannot be treated as strongly absorbing. A similar result applies for RESI. In contrast, SHIP OA emissions appeared to be more weakly absorbing than moderately absorbing, whereas TRAF emissions leaned toward weakly absorbing rather than very weakly absorbing. Very low k values were derived for OTHR sources, confirming their very low absorption properties. In summary, the obtained k values followed the following order: GFAS>RESI>TRAF>SHIP>OTHR.

Table 4.4. Imaginary refractive index of OA at 370nm derived for the different environments (REG: regional, SUB: suburban, URB: urban) and sources (GFAS, RESI, SHIP, TRAF, OTHR). Values averaged over the different sites used.

Environment	GFAS	RESI	SHIP	TRAF	OTHR
REG	0.0615	0.0451	0.0182	0.0122	0.0014
SUB	0.0398	0.0398	0.0049	0.0049	0.0012
URB	0.0934	0.0625	0.0314	0.0579	0.0081
ALL	0.0640	0.0481	0.0182	0.0218	0.003
ALL -– global	0.02				

Optimization of k across stations has underscored the complex, dynamic nature of OA light absorbing properties, influenced not only by emission sources but also by environmental conditions. Derived k values for total OA ranged from 0.005 (weakly absorbing) to 0.068 (weakly to moderately absorbing), indicating significant variability throughout Europe. This aligns with the existing knowledge that OA properties vary with composition, source, and atmospheric age (Cappa et al., 2011). Regional background stations such as MSY and HYY showed the lowest k values, consistent with their predominant biogenic SOA in these regions.

Optimizing k for OA sources revealed the significant impact of local and regional emissions on k values. In PAY, elevated k values were derived for GFAS and RESI sources (e.g., biomass, coal combustion), aligned with the known strong absorption characteristics of biomass burning aerosols (Zhang et al., 2020b; Pani et al., 2021). This is further supported by evidence suggesting that BrC from biomass burning can undergo significant dark chemical processing, affecting more than 70% of OA from this source (Kodros et al., 2020). Other regional stations such as HYY, OPE, RIG, and MSY showed the dominance of SOA from biogenic emissions, which explains their low k values (Zhao et al., 2015). In urban environments, TRAF emissions emerged as a significant contributor to light absorption, with derived k values (0.06) twice those reported for specific TRAF emissions (e.g., propane, diesel, gasoline) (Hossen et al., 2023; Lu et al., 2015), highlighting the complexity in urban environments. Stations near ports demonstrated the relevant SHIP contribution to OA light absorption, consistent with previous studies (Kapoor et al., 2023).

Figure 4.4 summarizes the impact of using the different k values optimized by stn or for all sites when calculating OA absorption considering source contribution (Case 4) and total OA mass (Case5) simulated by the model. In the figure we compare model results against all observational data used in this work. Case 5 represents the common approximation adopted by models in the literature to describe the optical properties of aerosol components, where a single k is assigned to each individual aerosol component before applying any mixing rule. Conversely, Case 4 introduces the refinement at the source level to investigate the benefit of exploiting the source information to describe absorption. The source-tagged method allows clearly the model to better account for the specific characteristics of OA source emissions at different sites, particularly in urban areas where sources of OA are more variable. In contrast, the non-source-tagged approach (Case 5) results in a broader range of errors, especially in higher-absorption environments such as urban and suburban areas.

The implementation of these source-specific k values significantly improves model agreement compared to using a constant k value for OA absorption (Case 5 all). The latter is actually a common practice in atmospheric models that typically adopt k value at 550 nm ranging from 0.005 to 0.006 (e.g. Tegen et al., 2019). This widespread modelling practice underscores the relevance of our findings, proposing a refined method for determining k values that could improve the accuracy of future estimates of BrC radiative forcing.

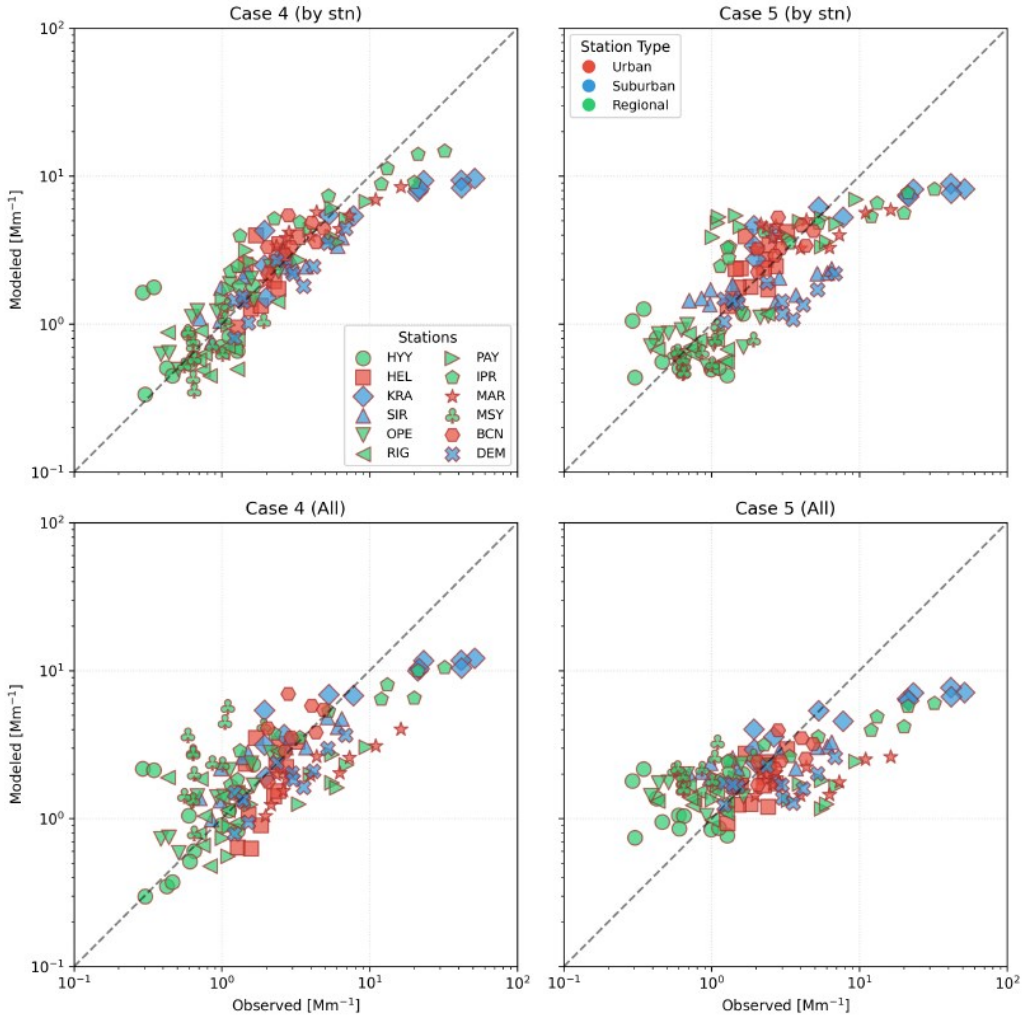

Figure 4.4: Monthly mean observed (abscissa) vs. modeled (ordinate) absorption for source contribution OA (Case 4) and total OA (Case 5) including optimization by 'stn' and 'all'. Symbols indicate individual stations and colors station type. Source: Navarro-Barboza et al. (2025).

4.2 Brown carbon representation in models: inter-annual variability in Europe

Atmospheric models usually treat OA as very weakly absorbing particles with no actual distinction between OA and BrC. As understanding of BrC in the atmosphere has improved, the representation of BrC in models has progressed from assuming a fraction of OA as strongly absorbing with a fixed imaginary refractive index (Park et al. 2010), classifying the absorption fraction of OA into different categories (Feng et al. 2013, Lin et al. 2014), to proposing and applying a parameterization of OA absorption from the ratio of emitted BC and OA based on experimental data (Saleh et al. 2014; 2015, Wang et al. 2018, Brown et al. 2018).

Regional studies provide detailed understanding into the BrC formation processes and their effects at the regional and local scale. Significant seasonal variations are found in BrC sources and concentrations where wildfire BB and residential wood burning are significantly impactful (Paraskevopoulou et al. 2023, Methymaki et al. 2023, Pani et al. 2021). Despite efforts over the past decade to include BrC in models (e.g., Wang et al. (2018), Brown et al. (2018), Zhang et al. (2020a)), several issues remain unaddressed regarding the observational and modeling aspects necessary to properly represent BrC, particularly their optical properties and emission sources (Samset et al., 2018; Saleh 2020).

Here, we analyze the intra-annual variability of the brown carbon (BrC) across Europe simulated by the MONARCH model accounting for biomass burning (BB) and biofuel (BF) BrC sources. A BrC scheme is implemented in the model to describe the absorption of primary BrC emissions that includes photobleaching effects. The model results are compared with in situ observations across Europe characterizing the absorption of BrC at 370nm (see Section 4.1.1). Sensitivity runs perturbing BrC emissions are analysed to investigate the uncertainties in the emission sources.

4.2.1 BrC parameterization

We have integrated a representation of BrC and emission sources derived from BB and BF emissions in the MONARCH model following Zhang et al. (2020a). The absorptivity of OA in BB and BF emissions can be parameterized as a function of the ratio of BC-to-OA emissions following Saleh et al. (2014). Based on this, the imaginary refractive index of OA (effective absorptivity; k_{OA}) is parameterized across diverse fuel types and burn conditions using the BC-to-OA ratio of emissions:

$$k_{OA,550} = 0.016 \log_{10} (E_{BC}/E_{OA}) + 0.03925$$

where $k_{OA,550}$ denotes the OA absorptivity at a wavelength of 550 nm. E_{BC} and E_{OA} are the emission rates of BC and OA, respectively, in $gm^{-2}\ s^{-1}$. This formulation allows for the computation of $k_{OA,550}$ as an intermediate step in calculating BrC emissions (E_{BrC}). For that, E_{BrC} are scaled as follows (Liu et al., 2013):

$$E_{BrC} = 4\pi k_{OA,550} \cdot EOA / (\rho \cdot 550nm \cdot MAE_{BrC}(550nm))$$

where ρ represents the density of the particles in gm^{-3}, E_{BrC} indicates the BrC emission rate in $gm^{-2}\ s^{-1}$, and $MAE_{BrC}(550nm)$ is the mass absorption efficiency of BrC. We assume a $MAE_{BrC}(550nm)$ value of 1 $m^2\ g^{-1}$ for primary BrC (McMeeking, 2008). The particle density of BrC is the same as that of OA in the model, 1800 kgm^{-3}.

In addition, we have implemented the "photobleaching effect" to account for the aging process of BrC particles, as photobleaching significantly changes their absorption properties. Forrister et al. (2015) has shown that 6% of the emitted BrC of BB and BF resist bleaching, while in Wang et al. (2018) and Neyestani and Saleh (2022) 25% of all BrC emissions are considered unchanged. Wong et al. (2019) found that up to 20% of BrC does not lose its light-absorbing properties, suggesting a minimum threshold for BrC light absorption that could be attributed to refractory and relatively inert BrC associated with macromolecules. In our simulation, we assume that 8% of the BrC retains its hydrophobic properties maintaining its absorbing properties, while the rest transitions to a hydrophilic state and possibly loses its absorption through a photobleaching process. This is an intermediate value among the reported in the literature and closer to Forrister et al. (2015). The photobleaching process is parametrised considering that BrC absorption in the model decreases with increasing concentration of hydroxyl radicals (OH) (Zhang et al., 2020a). The photobleaching is applied to 92% of the BrC emissions, as stated above, reflecting the proportion of primary BrC that undergoes the bleaching process. We only account

for BB and BF BrC sources, neglecting secondary production of BrC or other sources as those are still highly uncertain.

We use the optical package described in Section 4.1.1 to calculate the absorption of BrC from the mass of BrC simulated by the model and their optical and microphysical properties. The primary hydrophobic BrC that is not photobleached retains strongly absorption properties, while the photobleach fraction significantly losses absorption power. In this regard, we adopt a refractive imaginary index k = 0.129 for the primary emitted BrC (strongly absorbing) and k = 0.01 for the photobleached one (very weakly absorbing) following Saleh (2020) categorization. Note that k values are provided at 370 nm.

4.2.2 Emissions

The High-Elective Resolution Modelling Emission System version 3 (HERMESv3; Guevara et al. 2019) is used to process the anthropogenic and BB emissions to be used as input in the MONARCH model. We used emissions from BB and BF as main contributors to BrC. BB emissions are provided by the Global Fire Assimilation System version 1.2 (GFASv1.2) analysis accounting for forest, grassland, and agricultural waste fires.

Currently, there is a lack of emission inventories that quantify the emissions of carbonaceous species from BF sources in Europe at a spatial resolution suitable for our study. To address this limitation, we have combined information from the European-scale emission inventory CAMS-REG_v4.2 (Kuenen et al. 2022), developed under the Copernicus Atmosphere Monitoring Service (CAMS) which provides emissions for regulatory pollutants (CAMS-REG-AP_v4.2) and greenhouse gases (CAMS-REG-GHG_v4.2). CAMS-REG-GHG_v4.2 inventory reports emissions from fossil fuel and BF combustion sources. Based on this information, we have calculated the fraction of BF in total combustion emissions for each GNFR category at the country level and derive an average value per activity sector. The resulting BrC emissions derived from are shown in Figure 4.6. We estimate BrC emissions from BF sources to be approximately 0.30 Tg/yr and from BB sources 0.26 Tg/yr for 2018 in our European domain. Over Europe, Xiong et al. (2022) estimates a total BrC emission of 0.34 Tg/yr, with 38% attributed to BB sources and the rest to anthropogenic activities. These estimates align with the emissions used in our work, where we consider 64% higher emissions for Europe, totalling 0.56 Tg/yr.

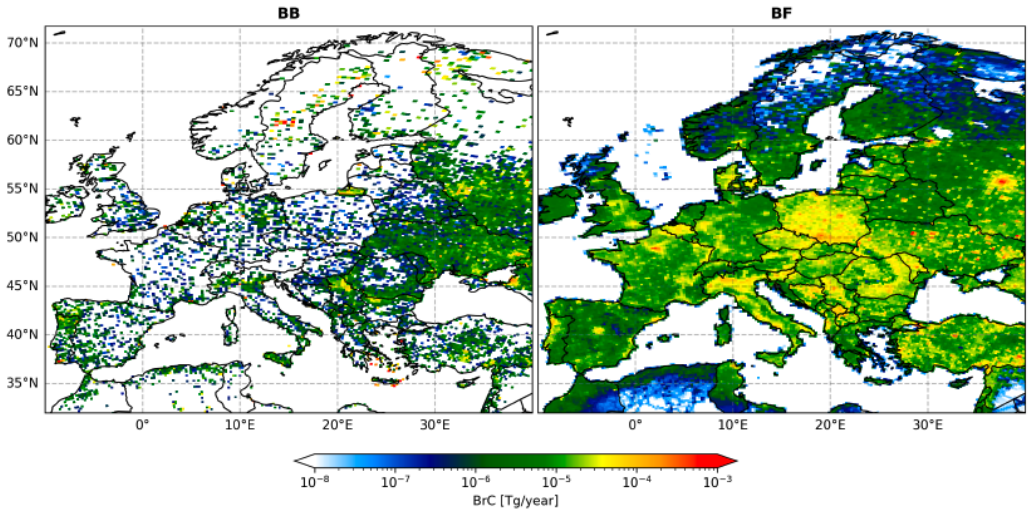

Figure 4.6: BrC emissions from BB and BF sources over Europe for 2018.

4.2.3 Results

The BrC results derived from the MONARCH simulation for 2018 over Europe significantly underestimates absorption observations at all locations, likely due to inaccurate description or lack of emissions. However, strong correlations are obtained at stations such as SIR and OPE, with PCC values of 0.72 and 0.73, respectively. Scaling emission sources (factor 7) significantly reduces the systematic bias. Figure 4.7 shows the comparison of OA absorption at surface compared with observations at the 12 European sites.

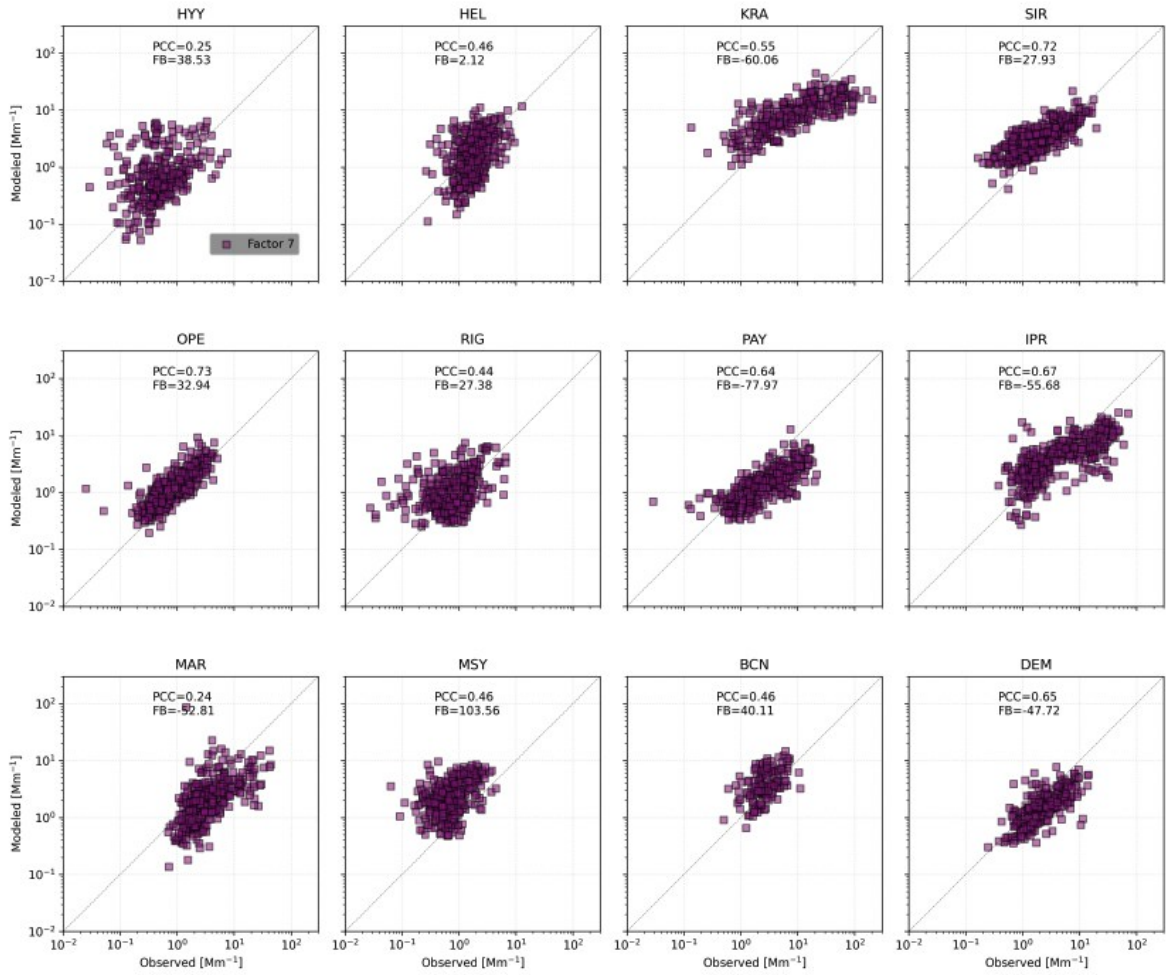

Figure 4.5: Comparison of daily mean observed and modelled OA absorption at 370 nm at twelve European sites for 2018.

Overall, the model captured reasonably well the temporal variability of BrC absorption across the study region. The model showed higher BrC absorption values during the colder months, which can be attributed to the increase in the use of biomass and biofuels for residential heating. In contrast, lower BrC absorption was observed during the warmer months, likely as a result of a combination of lower emissions and enhanced photobleaching effects. However, there were notable differences in the model performance across the various stations and some persistent biases were observed. In stations where biogenic SOA contribution dominates, such as the regional stations of MSY and HYY, low light absorption was observed, and the model exhibited

large overestimations when applying the scaling factor. This underscores the need for a refined treatment of BrC in regions dominated by SOA sources, taking into account the distinct optical properties of biogenic and anthropogenic SOA (Liu et al. 2016). Conversely, at stations such as PAY or KRA, the model underestimated absorption, even with the high scaling factor applied. This suggests that the emissions inputs at these sites may not be well-represented in the model and potentially relevant BrC sources like shipping emissions should be considered in future studies (Saleh 2020). In contrast, the model was able to reproduce the observed absorption levels relatively well at stations such as OPE and SIR.

The spatial distribution of BrC absorption is highly driven by residential emissions with hot-spot areas associated with large biomass burning emissions. The bleached BrC fraction simulated by the model arose as a secondary contributor compared with the strongly-absorbing primary BrC. Uncertainties in emissions and aging processes that affect BrC are still significant and more efforts are required to further improve the model results. However, statistical evaluation of the model results is consistent and aligned with the results discussed in Section 4.1, exemplifying the benefit of adopting specific BrC parameterization in numerical models. The enhanced understanding of BrC's role in atmospheric absorption can help to reduce the uncertainty of climate models. One limitation of our study is that the emission inventories may not accurately represent the emissions and more efforts are needed to develop consistent BrC emission inventories for future research.

5. SUMMARY

In this task we worked on the development and evaluation of climate and air quality models and the radiative effects of carbonaceous particles. The OpenIFS-HAM-M7 model was tested to provide further development targets for WP3. A machine learning-based parameterisation for cloud droplet concentrations was developed, with the goal of improving the representation of cloud-aerosol interactions in forthcoming OpenIFS versions. Sensitivity simulations were carried out with our models to assess the status of aerosol scheme development and exploring the uncertainties depending on model initialisation. These included global-scale simulations using the EC-Earth3 general circulation model, experimental simulations with the development version of OpenIFS-HAM-M7, simulations in European domain with the WRF model, and simulations with the MONARCH chemical transport model. In MONARCH, specific attention was given to testing and constraining the parameterisation of organic and brown carbon absorption. This was achieved through perturbation experiments and optimisation techniques designed to refine the optical properties of organic aerosols based on observational datasets. Especially for WRF the sensitivity studies provide valuable insights into how different configurations and parameter choices affect the simulations in WP6.

The climate model development and evaluation focused on OpenIFS-HAM-M7 and EC-Earth3, complemented by the development of a machine learning-based parameterisation. The OpenIFS-HAM-M7 model has been tested against surface observations of aerosol particle concentrations from ACTRIS stations. Initial results indicate that surface aerosol number concentrations are underpredicted, while simulated aerosol mass burdens are considerably higher, by a factor of 2 to 5, compared to values reported in the literature. Furthermore, the AOD was shown to be lower than that of MODIS satellite retrieval. Model development is continuing, with planned revision of wet deposition implementation for convective clouds to correct the aerosol removal and implementation of new particle formation. Simulations conducted with the EC-Earth3 model focused on assessing the climatic role of brown carbon and methyl sulfonic acid. While the global mean direct radiative effect of brown carbon appears to be negligible, regional impacts in areas such as China and Africa show a distinct influence on the local radiation budget. The MSA simulation shows how near the source regions CCN

at 0.2% supersaturation increases significantly. In parallel, a machine learning model has been developed to predict cloud droplet number concentrations based on gas, particle and meteorological predictors. The model shows rather good performance in environments represented in the training dataset, with 70 percent of predicted N100 values falling within a factor of 1.5 of observed values. This machine learning-based approach has strong potential for improving the run time of the model and treatment of aerosol-cloud interactions and is planned for testing in a future implementation into OpenIFS.

Regional-scale modelling efforts using the WRF and MONARCH models were utilised in this task, providing valuable insights into aerosol-climate interactions and model sensitivities. For WRF, a suite of sensitivity simulations was conducted to evaluate impact of model configurations on near-surface air temperature (T2m) performance. Preliminary analysis indicates that configurations S1a and S6 (see Table 3.1 for details) yield the best performance in reproducing observed T2m values. Among these, S6 is considered more suitable, as it uses continuous meteorological forcing, whereas the daily re-initialisation approach used in S1a, which, although it has good performance, is not applicable for long-term or climate-scale simulations. Further model evaluation is ongoing to assess performance across additional meteorological variables and observational datasets. Furthermore, MONARCH simulations have been used to investigate the behaviour of organic carbon and brown carbon absorption. Calculation of the absorption considering the source specific refractive index performs better than using a commonly used constant refractive index, therefore, models should preferably use the latter. The model captures the temporal variability of BrC absorption reasonably well. However, large uncertainties remain due to poorly constrained emission inventories and the complex ageing processes of organic aerosols. These findings underscore the need for specific BrC parameterisations in numerical models, which have the potential to significantly reduce uncertainties in the estimation of aerosol radiative effects. Improving emission inventories, particularly for organic aerosol sources and their evolution, will be essential for enhancing the accuracy of future climate projections.

6. OUTLOOK

OpenIFS-HAM-M7 Cy48r1 needs further evaluation and development for the underestimation of particle concentration and overestimations of aerosol burden and optical depths. Forthcoming improvements of NPF and convective wet deposition process in WP3 will provide immediate improvement here. EC-Earth3 sensitivity simulations showed that in certain cases, especially in China and Africa, the brown carbon has an impact, and it should be included in global climate models. Similarly, the MSA treatment is increasing CCN regionally and will be implemented in OpenIFS-HAM-M7/EC-Earth 4. A machine learning model developed to predict cloud droplet concentrations is planned for integration into OpenIFS to improve the cloud droplet predictions and model runtime. In regional modelling, WRF simulations identified the most suitable configuration for use in longer simulations. MONARCH simulations showed that 1) source specific refractive indices for organic aerosols should be used, 2) improving emission inventories, 3) ageing processes are needed and 4) dedicated model parameterisations should be implemented.

REFERENCES

Badia, A., Jorba, O., Voulgarakis, A., Dabdub, D., Pérez García-Pando, C., Hilboll, A., Gonçalves Ageitos, M., and Zavisa, J.: Description and evaluation of the Multiscale Online Nonhydrostatic AtmospheRe Chemistry model (NMMB-MONARCH) version 1.0: gas-phase chemistry at global scale, Geoscientific Model Development, 10, 609–638, 2017.

Bergman, T., Makkonen, R., Schrödner, R., Swietlicki, E., Phillips, V. T. J., Le Sager, P., and van Noije, T.: Description and evaluation of a secondary organic aerosol and new particle formation scheme within TM5-MP v1.2, Geosci. Model Dev., 15, 683–713, https://doi.org/10.5194/gmd-15-683-2022, 2022.

Brown, H., Liu, X., Feng, Y., Jiang, Y., Wu, M., Lu, Z., Wu, C., Murphy, S., and Pokhrel, R.: Radiative effect and climate impacts of brown carbon with the Community Atmosphere Model (CAM5), Atmospheric Chemistry and Physics, 18, 17 745–17 768, 2018.

Cappa, C.D., T. B. Onasch, P. Massoli, D. R. Worsnop, T. S. Bates, E. S. Cross, P. Davidovits, J. Hakala, K. L. Hayden, B. T. Jobson, et al. Radiative absorption enhancements due to the mixing state of atmospheric black carbon. Science, 337(6098):1078–1081, 2012.

Casotto, R., A. Skiba, M. Rauber, J. Strähl, A. Tobler, D. Bhattu, H. Lamkaddam, M. I. Manousakas, G. Salazar, T. Cui, et al. Organic aerosol sources in Krakow, Poland, before implementation of a solid fuel residential heating ban. Science of The Total Environment, 855:158655, 2023.

Coates, J., Mar, K. A., Ojha, N., and Butler, T. M. The influence of temperature on ozone production under varying NO_x conditions – a modelling study, Atmospheric Chemistry and Physics, 16, 11601–11615, https://doi.org/10.5194/acp-16-11601-2016., 2016

Debevec, C., Sauvage, S., Gros, V., Salameh, T., Sciare, J., Dulac, F., and Locoge, N. Seasonal variation and origins of volatile organic compounds observed during 2 years at a western Mediterranean remote background site (Ersa, Cape Corsica), Atmospheric Chemistry and Physics, 21, 1449–1484, https://doi.org/10.5194/acp-21-1449-2021., 2021

Du, Q., Zhao, C., Zhang, M., Dong, X., Chen, Y., Liu, Z., Hu, Z., Zhang, Q., Li, Y., Yuan, R., and Miao, S. Modeling diurnal variation of surface PM2.5 concentrations over East China with WRF-Chem: impacts from boundary-layer mixing and anthropogenic emission, Atmospheric Chemistry and Physics, 20, 2839–2863, https://doi.org/10.5194/acp-20-2839-2020., 2020

EPA, 2025. U.S. Environmental Protection Agency. Technical Overview of Volatile Organic Compounds. Available from: https://www.epa.gov/indoor-air-quality-iaq/technical-overview-volatile-organic-compounds.

Fang, W., Andersson, A., Lee, M. et al. Combined influences of sources and atmospheric bleaching on light absorption of water-soluble brown carbon aerosols. Npj Clim Atmos Sci 6, 104, https://doi.org/10.1038/s41612-023-00438-8, 2023

Feng, Y., Ramanathan, V., and Kotamarthi, V.: Brown carbon: a significant atmospheric absorber of solar radiation?, Atmospheric Chemistry and Physics, 13, 8607–8621, 2013.

Forrister, H., Liu, J., Scheuer, E., Dibb, J., Ziemba, L., Thornhill, K. L., Anderson, B., Diskin, G., Perring, A. E., Schwarz, J. P., et al.: Evolution of brown carbon in wildfire plumes, Geophysical Research Letters, 42, 4623–4630, 2015.

Gliß, J., Mortier, A., Schulz, M., Andrews, E., Balkanski, Y., Bauer, S. E., Benedictow, A. M. K., Bian, H., Checa-Garcia, R., Chin, M., Ginoux, P., Griesfeller, J. J., Heckel, A., Kipling, Z., Kirkevåg, A., Kokkola, H.,

Laj, P., Le Sager, P., Lund, M. T., Lund Myhre, C., Matsui, H., Myhre, G., Neubauer, D., van Noije, T., North, P., Olivié, D. J. L., Rémy, S., Sogacheva, L., Takemura, T., Tsigaridis, K., and Tsyro, S. G.: AeroCom phase III multi-model evaluation of the aerosol life cycle and optical properties using ground- and space-based remote sensing as well as surface in situ observations, Atmos. Chem. Phys., 21, 87–128, https://doi.org/10.5194/acp-21-87-2021, 2021.

Granier, C., Darras, S., van der Gon, H. D., Jana, D., Elguindi, N., Bo, G., Michael, G., Marc, G., Jalkanen, J.-P., Kuenen, J., et al.: The Copernicus atmosphere monitoring service global and regional emissions (April 2019 version), Ph.D. thesis, Copernicus Atmosphere Monitoring Service, 2019.

Guenther, A., Karl, T., Harley, P., Wiedinmyer, C., Palmer, P. I., and Geron, C.: Estimates of global terrestrial isoprene emissions using MEGAN (Model of Emissions of Gases and Aerosols from Nature), Atmospheric Chemistry and Physics, 6, 3181–3210, https://doi.org/10.5194/acp-6-3181-2006, 2006.

Guevara, M., Tena, C., Porquet, M., Jorba, O., and Pérez García-Pando, C.: HERMESv3, a stand-alone multi-scale atmospheric emission modelling framework–Part 1: global and regional module, Geoscientific Model Development, 12, 1885–1907, 2019.

Gultepe, I., and Isaac, G. A.: Scale Effects on Averaging of Cloud Droplet and Aerosol Number Concentrations: Observations and Models. J. Climate, 12, 1268–1279, 1999.

Gupta, P., Payra, S., Bhatla, R., Verma, S. WRF-Chem 31Modelling study of heat wave driven ozone over southeast region, India, Environmental Pollution, 340 (2), 122744. https://doi.org/10.1016/j.envpol.2023.122744., 2024

Hersbach, Hans, et al. The ERA5 global reanalysis., Quarterly journal of the royal meteorological society 146.730, 1999-2049. **https://doi.org/10.1002/qj.3803**, 2023

Ho, D., Gałkowski, M., Reum, F., Botía, S., Marshall, J., Totsche, K. U., and Gerbig, C. Recommended coupling to global meteorological fields for long-term tracer simulations with WRF-GHG, Geoscientific Model Development, 17, 7401–7422, https://doi.org/10.5194/gmd-17-7401-2024., 2024

Hoffmann, P., Reinhart, V., Rechid, D. LUCAS LUC future land use and land cover change dataset for Europe (Version 1.1). World Data Center for Climate (WDCC) at DKRZ., https://doi.org/10.26050/WDCC/LUC_future_EU_v1.1., 2022a

Hoffmann, P., Reinhart, V., Rechid, D. LUCAS LUC historical land use and land cover change dataset for Europe (Version 1.1). World Data Center for Climate (WDCC) at DKRZ. , https://doi.org/10.26050/WDCC/LUC_hist_EU_v1.1., 2022b

Hodshire, A. L., Campuzano-Jost, P., Kodros, J. K., Croft, B., Nault, B. A., Schroder, J. C., Jimenez, J. L., and Pierce, J. R.: The potential role of methanesulfonic acid (MSA) in aerosol formation and growth and the associated radiative forcings, Atmos. Chem. Phys., 19, 3137–3160, https://doi.org/10.5194/acp-19-3137-2019, 2019.

Hoesly, R. M., Smith, S. J., Feng, L., Klimont, Z., Janssens-Maenhout, G., Pitkanen, T., Seibert, J. J., Vu, L., Andres, R. J., Bolt, R. M., Bond, T. C., Dawidowski, L., Kholod, N., Kurokawa, J.-I., Li, M., Liu, L., Lu, Z., Moura, M. C. P., O'Rourke, P. R., and Zhang, Q.: Historical (1750–2014) anthropogenic emissions of reactive gases and aerosols from the Community Emissions Data System (CEDS), Geosci. Model Dev., 11, 369–408, https://doi.org/10.5194/gmd-11-369-2018, 2018.

Hossen, M. A.-a., Roy, S., Zaman, S. U., and Salam, A.: Emission of water soluble brown carbon from different combustion sources: optical properties and functional group characterisation, Environmental Research Communications, 5, 081 002, 2023.

Huijnen, V., Williams, J., van Weele, M., van Noije, T., Krol, M., Dentener, F., Segers, A., Houweling, S., Peters, W., de Laat, J., Boersma, F., Bergamaschi, P., van Velthoven, P., Le Sager, P., Eskes, H., Alkemade, F., Scheele, R., Nédélec, P., and Pätz, H.-W.: The global chemistry transport model TM5: description and evaluation of the tropospheric chemistry version 3.0, Geosci. Model Dev., 3, 445–473, https://doi.org/10.5194/gmd-3-445-2010, 2010.

Huijnen, V., Le Sager, P., Köhler, M. O., Carver, G., Rémy, S., Flemming, J., Chabrillat, S., Errera, Q., and van Noije, T.: OpenIFS/AC: atmospheric chemistry and aerosol in OpenIFS 43r3, Geosci. Model Dev., 15, 6221–6241, https://doi.org/10.5194/gmd-15-6221-2022, 2022.

Jeon, W., Choi, Y., Lee, H, W., Lee, S., Yoo, J., Park, J., Lee, H. A quantitative analysis of grid nudging effect on each process of PM2.5 production in the Korean Peninsula, Atmospheric Environment, 122, 763-774. https://doi.org/10.1016/j.atmosenv.2015.10.050., 2015

Kaiser, J., Heil, A., Andreae, M., Benedetti, A., Chubarova, N., Jones, L., Morcrette, J.-J., Razinger, M., Schultz, M., Suttie, M., et al.: Biomass burning emissions estimated with a global fire assimilation system based on observed fire radiative power, Biogeosciences, 9, 527–554, 2012.

Kapoor, T. S., Phuleria, H. C., Sumlin, B., Shetty, N., Anurag, G., Bansal, M., Duhan, S. S., Khan, M. S., Laura, J. S., Manwani, P., et al.: Optical Properties and Refractive Index of Wintertime Aerosol at a Highly Polluted North-Indian Site, Journal of Geophysical Research: Atmospheres, 128, e2022JD038 272, 2023.

Klose, M., Jorba, O., Gonçalves Ageitos, M., Escribano, J., Dawson, M. L., Obiso, V., Di Tomaso, E., Basart, S., Montané Pinto, G., Macchia, F., et al.: Mineral dust cycle in the Multiscale Online Nonhydrostatic AtmospheRe CHemistry model (MONARCH) version 2.0, Geoscientific Model Development, 14, 6403–6444, 2021.

Kodros, J., Papanastasiou, D., Paglione, M., Masiol, M., Squizzato, S., Florou, K., Kołodziejczyk, A., Skyllakou, K., Nenes, A., and Pandis, S.: The oxidizing power of the dark side: Rapid nocturnal aging of biomass burning as an overlooked source of oxidized organic aerosol, in: EGU General Assembly Conference Abstracts, EGU General Assembly Conference Abstracts, p. 7382, 2020.

Kuenen, J., Dellaert, S., Visschedijk, A., Jalkanen, J.-P., Super, I., and Denier van der Gon, H.: CAMS-REG-v4: a state-of-the-art highresolution European emission inventory for air quality modelling, Earth System Science Data, 14, 491–515, 2022.

Laj, P., Lund Myhre, C., Riffault, V., Amiridis, V., Fuchs, H., Eleftheriadis, K., Petäjä, T., Salameh, T., Kivekäs, N., Juurola, E., Saponaro, G., Philippin, S., Cornacchia, C., Alados Arboledas, L., Baars, H., Claude, A., De Mazière, M., Dils, B., Dufresne, M., Evangeliou, N., Favez, O., Fiebig, M., Haeffelin, M., Herrmann, H., Höhler, K., Illmann, N., Kreuter, A., Ludewig, E., Marinou, E., Möhler, O., Mona, L., Eder Murberg, L., Nicolae, D., Novelli, A., O'Connor, E., Ohneiser, K., Petracca Altieri, R. M., Picquet-Varrault, B., van Pinxteren, D., Pospichal, B., Putaud, J., Reimann, S., Siomos, N., Stachlewska, I., Tillmann, R., Voudouri, K. A., Wandinger, U., Wiedensohler, A., Apituley, A., Comerón, A., Gysel-Beer, M., Mihalopoulos, N., Nikolova, N., Pietruczuk, A., Sauvage, S., Sciare, J., Skov, H., Svendby, T., Swietlicki, E., Tonev, D., Vaughan, G., Zdimal, V., Baltensperger, U., Doussin, J., Kulmala, M., Pappalardo, G., Sorvari Sundet, S., & Vana, M. Aerosol, Clouds and Trace Gases Research Infrastructure (ACTRIS): The European Research Infrastructure

Supporting Atmospheric Science. *Bulletin of the American Meteorological Society*, *105*(7), E1098-E1136. https://doi.org/10.1175/BAMS-D-23-0064.1 , 2024

Laskin, A., Laskin, J., and Nizkorodov, S. A.: Chemistry of atmospheric brown carbon, Chemical reviews, 115, 4335–4382, 2015.

S. Li, H. Zhang, Z.Wang, Y. Chen, et al. Advances in the research on brown carbon aerosols: Its concentrations, radiative forcing, and effects on climate. Aerosol and Air Quality Research, 23(8):220336, 2023.

Lin, G., Penner, J. E., Flanner, M. G., Sillman, S., Xu, L., and Zhou, C.: Radiative forcing of organic aerosol in the atmosphere and on snow: Effects of SOA and brown carbon, Journal of Geophysical Research: Atmospheres, 119, 7453–7476, 2014.

Liu, J., M. Bergin, H. Guo, L. King, N. Kotra, E. Edgerton, and R. Weber. Sizeresolved measurements of brown carbon in water and methanol extracts and estimates of their contribution to ambient fine-particle light absorption. Atmospheric Chemistry and Physics, 13(24):12389–12404, 2013.

Liu, J., P. Lin, A. Laskin, J. Laskin, S. M. Kathmann, M. Wise, R. Caylor, F. Imholt, V. Selimovic, and J. E. Shilling. Optical properties and aging of light-absorbing secondary organic aerosol. Atmos. Chem. Phys, 16(19):12815–12827, 2016.

Lu, Z., Streets, D. G., Winijkul, E., Yan, F., Chen, Y., Bond, T. C., Feng, Y., Dubey, M. K., Liu, S., Pinto, J. P., et al.: Light absorption properties and radiative effects of primary organic aerosol emissions, Environmental science & technology, 49, 4868–4877, 2015.

McMeeking, G.R. The optical, chemical, and physical properties of aerosols and gases emitted by the laboratory combustion of wildland fuels. Colorado State University, 2008.

Methymaki, G., E. Bossioli, D. Boucouvala, A. Nenes, and M. Tombrou. Brown carbon absorption in the mediterranean basin from local and long-range transported biomass burning air masses. Atmospheric Environment, 306:119822, 2023.

Mishchenko, M. I., Travis, L. D., and Lacis, A. A.: Scattering, absorption, and emission of light by small particles, Cambridge university press, 2002.

Navarro-Barboza, H., Pandolfi, M., Guevara, M., Enciso, S., Tena, C., Via, M., Yus-Díez, J., Reche, C., Pérez, N., Alastuey, A., et al.: Uncertainties in source allocation of carbonaceous aerosols in a Mediterranean region, Environment international, 183, 108 252, 2024.

Navarro-Barboza, H., Rovira, J., Obiso, V., Pozzer, A., Via, M., Alastuey, A., Querol, X., Perez, N., Savadkoohi, M., Chen, G., Yus-Díez, J., Ivancic, M., Rigler, M., Eleftheriadis, K., Vratolis, S., Zografou, O., Gini, M., Chazeau, B., Marchand, N., Prevot, A., Dallenbach, K., Ehn, M., Luoma, K., Petäjä, T., Tobler, A., Necki, J., Aurela, M., Timonen, H., Niemi, J., Favez, O., Petit, J.-E., Putaud, J.-P., Hueglin, C., Pascal, N., Chauvigné, A., Conil, S., Pandolfi, M., and Jorba, O.: Characterization of Brown Carbon absorption in different European environments through source contribution analysis, EGUsphere [accepted], https://doi.org/10.5194/egusphere-2024-2086, 2025.

National Centers for Environmental Prediction/National Weather Service/NOAA/U.S. Department of Commerce (2000): NCEP FNL Operational Model Global Tropospheric Analyses, continuing from July 1999. Research Data Archive at the National Center for Atmospheric Research, Computational and Information Systems Laboratory. https://doi.org/10.5065/D6M043C6. Accessed 14-08-2025.

Neyestani, S. E. and Saleh, R.: Observationally constrained representation of brown carbon emissions from wildfires in a chemical transport model, Environmental Science: Atmospheres, 2, 192–201, 2022.

Obiso, V.: Assessment of dynamic aerosol-radiation interaction in atmospheric models, Universitat Politècnica de Catalunya, 2018.

Pai, S. J., Heald, C. L., Pierce, J. R., Farina, S. C., Marais, E. A., Jimenez, J. L., Campuzano-Jost, P., Nault, B. A., Middlebrook, A. M., Coe, H., Shilling, J. E., Bahreini, R., Dingle, J. H., and Vu, K.: An evaluation of global organic aerosol schemes using airborne observations, Atmos. Chem. Phys., 20, 2637–2665, https://doi.org/10.5194/acp-20-2637-2020, 2020.

Pani, S. K., Lin, N.-H., Griffith, S. M., Chantara, S., Lee, C.-T., Thepnuan, D., and Tsai, Y. I.: Brown carbon light absorption over an urban environment in northern peninsular Southeast Asia, Environmental Pollution, 276, 116 735, 2021.

Paraskevopoulou, D., Kaskaoutis, D., Grivas, G., Bikkina, S., Tsagkaraki, M., Vrettou, I., Tavernaraki, K., Papoutsidaki, K., Stavroulas, I., Liakakou, E., et al.: Brown carbon absorption and radiative effects under intense residential wood burning conditions in Southeastern Europe: New insights into the abundance and absorptivity of methanol-soluble organic aerosols, Science of The Total Environment, 860, 160 434, 2023.

Parra, R. Effect of Global Atmospheric Datasets in Modelling Meteorology and Air Quality in the Andean Region of Ecuador, Aerosol and Air Quality Research, 22, 210292., https://doi.org/10.4209/aaqr.210292., 2022

Parker, W. S. Reanalyses and Observations: What's the Difference? Bulletin of the American Meteorological Society, 97, 1565–1572, https://doi.org/10.1175/BAMS-D-14-00226.1., 2016

Park, R. J., Kim, M. J., Jeong, J. I., Youn, D., and Kim, S.: A contribution of brown carbon aerosol to the aerosol light absorption and its radiative forcing in East Asia, Atmospheric Environment, 44, 1414–1421, 2010.

Payra, S., Gupta, P., Sarkar, A., Bhatla, R., Verma, S. Changes in tropospheric ozone concentration over Indo-Gangetic Plains: the role of meteorological parameters. Meteorology and Atmospheric Physics, 134, 96. https://doi.org/10.1007/s00703-022-00932-3., 2022

Qin, Y. M., Tan, H. B., Li, Y. J., Li, Z. J., Schurman, M. I., Liu, L., Wu, C., and Chan, C. K.: Chemical characteristics of brown carbon in atmospheric particles at a suburban site near Guangzhou, China, Atmospheric Chemistry and Physics, 18, 16 409–16 418, 2018.

Rosenfeld, D., Andreae, M. O., Asmi, A., Chin, M., Leeuw, G., Donovan, D. P., Kahn, R., Kinne, S., Kivekäs, N., Kulmala, M., Lau, W., Schmidt, K. S., Suni, T., Wagner, T., Wild, M., & Quaas, J. Global observations of aerosol-cloud-precipitation- climate interactions. Rev. Geophys., 52, 750–808., 2014

Saleh, R., Robinson, E. S., Tkacik, D. S., Ahern, A. T., Liu, S., Aiken, A. C., Sullivan, R. C., Presto, A. A., Dubey, M. K., Yokelson, R. J., et al.: Brownness of organics in aerosols from biomass burning linked to their black carbon content, Nature Geoscience, 7, 647–650, 2014.

Saleh, R., Marks, M., Heo, J., Adams, P. J., Donahue, N. M., and Robinson, A. L.: Contribution of brown carbon and lensing to the direct radiative effect of carbonaceous aerosols from biomass and biofuel burning emissions, Journal of Geophysical Research: Atmospheres, 120, 10–285, 2015.

Saleh, R.: From measurements to models: toward accurate representation of brown carbon in climate calculations, Current Pollution Reports, 6, 90–104, 2020.

Samset, B.H., C.W. Stjern, E. Andrews, R. A. Kahn, G. Myhre, M. Schulz, and G. L. Schuster. Aerosol absorption: Progress towards global and regional constraints. Current climate change reports, 4:65–83, 2018.

Santos-Alamillos, F. J., Pozo-Vázquez, D., Ruiz-Arias, J. A., Lara-Fanego, V., Tovar-Pescador, J. Analysis of WRF Model Wind Estimate Sensitivity to Physics Parameterization Choice and Terrain Representation in Andalusia (Southern Spain). Journal of Applied Meteorology and Climatology, 52, 1592–1609, https://doi.org/10.1175/JAMC-D-12-0204.1.,2013

M. Spada, O. Jorba, C. Pérez García-Pando, Z. Janjic, and J. Baldasano. Modeling and evaluation of the global sea-salt aerosol distribution: sensitivity to size resolved and sea-surface temperature dependent emission schemes. Atmospheric Chemistry and Physics, 13(23):11735–11755, 2013.

M. Spada. Development and evaluation of an atmospheric aerosol module implemented within the NMMB/BSC-CTM. PhD thesis, Universitat Politècnica de Catalunya, 2015.

Stergiou, I., Tagaris, E., Sotiropoulou, R.-E. P. Sensitivity Assessment of WRF Parameterizations over Europe. Proceedings, 1(5), 119. , https://doi.org/10.3390/ecas2017-04138., 2017

Stohl, A., Aamaas, B., Amann, M., Baker, L. H., Bellouin, N., Berntsen, T. K., Boucher, O., Cherian, R., Collins, W., Daskalakis, N., Dusinska, M., Eckhardt, S., Fuglestvedt, J. S., Harju, M., Heyes, C., Hodnebrog, Ø., Hao, J., Im, U., Kanakidou, M., Klimont, Z., Kupiainen, K., Law, K. S., Lund, M. T., Maas, R., MacIntosh, C. R., Myhre, G., Myriokefalitakis, S., Olivié, D., Quaas, J., Quennehen, B., Raut, J.-C., Rumbold, S. T., Samset, B. H., Schulz, M., Seland, Ø., Shine, K. P., Skeie, R. B., Wang, S., Yttri, K. E., and Zhu, T.: Evaluating the climate and air quality impacts of short-lived pollutants, Atmos. Chem. Phys., 15, 10529–10566, https://doi.org/10.5194/acp-15-10529-2015, 2015.

Tegen, I., Neubauer, D., Ferrachat, S., Siegenthaler-Le Drian, C., Bey, I., Schutgens, N., Stier, P., Watson-Parris, D., Stanelle, T., Schmidt, H., et al.: The global aerosol–climate model ECHAM6. 3–HAM2. 3–Part 1: Aerosol evaluation, Geoscientific Model Development, 12, 1080 1643–1677, 2019.

van Marle, M. J. E., Kloster, S., Magi, B. I., Marlon, J. R., Daniau, A.-L., Field, R. D., Arneth, A., Forrest, M., Hantson, S., Kehrwald, N. M., Knorr, W., Lasslop, G., Li, F., Mangeon, S., Yue, C., Kaiser, J. W., and van der Werf, G. R.: Historic global biomass burning emissions for CMIP6 (BB4CMIP) based on merging satellite observations with proxies and fire models (1750–2015), Geosci. Model Dev., 10, 3329–3357, https://doi.org/10.5194/gmd-10-3329-2017, 2017.

Vignati, E., Wilson, J., and Stier, P.: M7: An efficient size-resolved aerosol microphysics module for large-scale aerosol transport models, J. Geophys. Res., 109, D22202, https://doi.org/10.1029/2003JD004485, 2004.

Wang, L., Li, Z., Tian, Q., Ma, Y., Zhang, F., Zhang, Y., Li, D., Li, K., and Li, L.: Estimate of aerosol absorbing components of black carbon, brown carbon, and dust from ground-based remote sensing data of sun-sky radiometers, Journal of Geophysical Research: Atmospheres, 118, 6534–6543, 2013.

Wang, X., Heald, C. L., Liu, J.,Weber, R. J., Campuzano-Jost, P., Jimenez, J. L., Schwarz, J. P., and Perring, A. E.: Exploring the observational constraints on the simulation of brown carbon, AGU, 2018.

Wong, J. P., Tsagkaraki, M., Tsiodra, I., Mihalopoulos, N., Violaki, K., Kanakidou, M., Sciare, J., Nenes, A., and Weber, R. J.: Atmospheric evolution of molecular-weight-separated brown carbon from biomass burning, Atmospheric Chemistry and Physics, 19, 7319–7334, 2019.

Xiong, R., Li, J., Zhang, Y., Zhang, L., Jiang, K., Zheng, H., Kong, S., Shen, H., Cheng, H., Shen, G., et al.: Global brown carbon emissions from combustion sources, Environmental Science and Ecotechnology, 12, 100 201, 2022.

Zhang, A.,Wang, Y., Zhang, Y.,Weber, R. J., Song, Y., Ke, Z., and Zou, Y.:Modeling the global radiative effect of brown carbon: a potentially larger heating source in the tropical free troposphere than black carbon, Atmospheric Chemistry and Physics, 20, 1901–1920, 2020a.

Zhang, Y., Albinet, A., Petit, J.-E., Jacob, V., Chevrier, F., Gille, G., Pontet, S., Chrétien, E., Dominik-Sègue, M., Levigoureux, G., et al.: Substantial brown carbon emissions from wintertime residential wood burning over France, Science of the Total Environment, 743, 140 752, 2020b.

Zhao, R., Lee, A. K., Huang, L., Li, X., Yang, F., and Abbatt, J. P.: Photochemical processing of aqueous atmospheric brown carbon, Atmospheric Chemistry and Physics, 15, 6087–6100, 2015.

Appendix

Table A1. T2m statistical metrics from 9 sensitivity simulations (annual averaged data over 115 stations).

	FAC2	MB	MGE	NMB	NMGE	RMSE	r	r^2	p-value	COE	IOA
S1a	0.98	-1.14	1.14	-0.09	0.09	1.20	1.00	1.00	0.00	0.81	0.90
S1b	0.91	-2.05	2.12	-0.17	0.17	2.42	0.98	0.97	0.00	0.64	0.82
S2	0.92	-2.34	2.38	-0.18	0.19	2.76	0.98	0.96	0.00	0.59	0.80
S3	0.92	-1.96	2.09	-0.16	0.17	2.38	0.98	0.96	0.00	0.65	0.82
S4a	0.92	-2.28	2.39	-0.18	0.19	2.82	0.97	0.94	0.00	0.60	0.80
S4b	0.90	-2.34	2.44	-0.19	0.20	2.78	0.98	0.95	0.00	0.59	0.79
S5a	0.87	-2.46	2.49	-0.20	0.20	2.85	0.98	0.96	0.00	0.58	0.79
S5b	0.89	-2.21	2.25	-0.18	0.18	2.46	0.99	0.97	0.00	0.62	0.81
S6	0.98	-1.25	1.25	-0.10	0.1	1.28	1.00	1.00	0.00	0.79	0.90

Table A2. T2m maximum, minimum, mean, median, standard deviation and data range from observations and numerical results (annual averaged over all stations). Bias values (model – observation) presented in parentheses for S1a, S3, S5b and S6.

	Max	Min	Mean	Median	Range (Max - Min)	Standard Deviation
OBS	24.37	-3.18	12.39	12.63	27.55	6.71
S1a	22.88 (-1.5)	-4.34 (-1.2)	11.25 (-1.2)	11.42 (-1.2)	27.22	6.48
S1b	21.42	-5.46	10.34	10.31	26.88	6.2
S2	21.86	-5.22	10.03	9.85	27.08	5.99
S3	21.99 (-2.4)	-5.31 (-2.1)	10.11 (-2.3)	9.77 (-2.9)	27.3	5.96
S4a	22.13	-6.56	9.93	9.82	28.69	6.98
S4b	21.12	-6.29	10.05	9.82	27.4	6.26
S5a	22.13	-6.56	9.91	9.78	28.69	6.98
S5b	22.15 (-2.2)	-6.32 (-3.1)	10.18 (-2.2)	9.82 (-2.8)	28.48	6.66
S6	22.93 (-1.4)	-4.23 (-1.1)	11.15 (-1.2)	11.41 (-1.2)	27.16	6.63